Available online at www.sciencedirect.com
SCIENCE DIRECT®
Journal of Computational Physics 193 (2004) 595–619
JOURNAL OF COMPUTATIONAL PHYSICS
www.elsevier.com/locate/jcp

Truncation error analysis of lattice Boltzmann methods

David J. Holdych [a,b], David R. Noble [c,*], John G. Georgiadis [a,b], Richard O. Buckius [a]

[a] Department of Mechanical and Industrial Engineering, University of Illinois at Urbana-Champaign, Urbana, IL 61801, USA
[b] NSF Science and Technical Center of Advanced Materials for the Purification of Water with Systems, USA
[c] Sandia National Laboratories, Albuquerque, NM 87185-0826, USA

Received 12 March 2002; received in revised form 22 August 2003; accepted 29 August 2003

Abstract

A truncation error analysis is performed for models based on the lattice Boltzmann (LB) equation. This analysis involves two steps: the recursive application of the LB equation and a Taylor series expansion. Unlike previous analytical studies of LB methods, the present work does not assume an asymptotic relationship between the temporal and spatial discretization parameters or between the probability distribution function, f, and its equilibrium distribution, f^{eq}. Effective finite difference stencils are derived for both the distribution function and the primitive variables, i.e., density and velocity. The governing partial differential equations are also recovered. The associated truncation errors are derived and the results are validated by numerical simulation of analytic flows. Analysis of the truncation errors elucidates the roles of the kinetic theory relaxation parameter, τ, and the discretization parameters, Δx and Δt. The effects of initial and boundary conditions are also addressed and are shown to significantly affect the overall accuracy of the method.

Keywords: Lattice Boltzmann; Truncation error; Chapman–Enskog; Finite difference

1. Introduction

The lattice Boltzmann (LB) method was originally developed as a natural extension to the lattice gas method for modeling fluid flow based upon kinetic theory [3,17–19,29]. These fluid flow models have been used to simulate formidable problems such as flows of suspensions [26] and porous media flows [28,35]. Additionally, LB models have been developed to simulate multiphase and multicomponent flows [12,20,33,36].

Conservation equations in the LB method are formulated in terms of intermediate variables, f_j. These intermediate variables propagate in discrete lattice directions, $\mathbf{w}_j$, and evolve according to the lattice

* Corresponding author. Tel.: +1-505-844-2274; fax: +1-505-844-8251.
E-mail address: drnoble@sandia.gov (D.R. Noble).

0021-9991/$ - see front matter © 2003 Elsevier B.V. All rights reserved.
doi:10.1016/j.jcp.2003.08.012

Boltzmann equation. Here, the focus is placed on the most common form of the LB equation, which uses the Bhatnagar–Gross–Krook [4] model:

$$f_j(\mathbf{x} + \Delta x \mathbf{w}_j, t + \Delta t) = f_j(\mathbf{x}, t) - \frac{1}{\tau}\left[f_j(\mathbf{x}, t) - f_j^{\mathrm{eq}}(\mathbf{x}, t)\right], \tag{1}$$

where Δx and Δt are the spatial and temporal discretizations, respectively, f_j^{eq} is an equilibrium state for f_j, and τ is a dimensionless relaxation parameter corresponding to the dimensional relaxation time divided by Δt. Primitive variables, such as density and momentum, are determined from moments or linear combinations of f_j with respect to $\mathbf{w}_j$. In turn, f_j^{eq} is specified in terms of the primitive variables.

Evolution equations corresponding to the LB method have been derived in the past with a variety of techniques. The equations governing LB fluid flow models were first obtained using the Chapman–Enskog asymptotic procedure [11]. In this procedure, a non-dimensional form of Eq. (1) is converted into an asymptotic form by writing $\Delta x = c\Delta t$, where $c \equiv \Delta x/\Delta t$, and by introducing three expansions in terms of a small non-dimensional time step ε. These expansions include a Taylor series expansion of $f_j(\mathbf{x} + c\mathbf{w}_j\Delta t, t + \Delta t)$ about $f_j(\mathbf{x}, t)$, an asymptotic expansion of f_j about f_j^{eq}, and an asymptotic expansion of time. When the appropriate moments are applied to the resulting equation, the LB fluid models are found to satisfy both the continuity and Navier–Stokes equations if the dimensional viscosity is defined as $v \propto (2\tau - 1)\Delta x^2/\Delta t$. Swift et al. [36] introduced a more straightforward method for analyzing LB fluid models that eliminates the need for multiple time scales. In their analysis, a Taylor series analysis of $f_j(\mathbf{x} + c\mathbf{w}_j\Delta t, t + \Delta t)$ about $f_j(\mathbf{x}, t)$ is introduced into Eq. (1), and f_j is obtained in terms of f_j^{eq} and derivatives of f_j^{eq} through successive approximation. Another analytical procedure that avoids the need for multiple time scales was introduced by Junk [22]. In this procedure, the lattice Boltzmann equation is reduced to a solvable differential form by introducing the diffusion scaling, $\Delta t = \varepsilon^2 = \Delta x^2$, in a Taylor series expansion of Eq. (1).

Connections between the LB method and finite difference methods have been made by a number of authors [1,9,22]. Ancona [1] examined the similarities between the LB formulation and the formulation of other fully Lagrangian schemes. More recently, Junk [22] analyzed how each of the Navier–Stokes differential operators are approximated in the LB method. Additionally, Junk demonstrated that the LB method can be viewed as a "linear combination of a direct and a relaxation scheme." Based upon Junk's analysis, Junk and Klar [23] derived a finite difference scheme which uses approximations for the differential operators that are similar to those of the LB method.

The Chapman–Enskog procedure has been used successfully to recover the continuity and Navier–Stokes equations. However, errors of the LB fluids model have only been explicitly reported through the same order as the viscous term, $O(\varepsilon)$, with additional terms only denoted as $O(\varepsilon^2)$ [21]. These analytical studies have been truncated at this order due in part to the cumbersome use of multiple time scales in the Chapman–Enskog procedure. As a result, numerical studies of the LB method have been the main source for determining the method's convergence, indicating that the method exhibits second-order spatial accuracy when τ is held constant [2,31,34]. Skordos [34] found that the method demonstrates second-order temporal accuracy when the grid is fixed. However, Reider and Sterling [32] found that the temporal convergence of the LB method is effectively first order when reducing all error terms consistently, and this finding can also be supported based on results of Junk's study [22].

There are two open issues on the lattice Boltzmann method that are considered in this paper. The first issue concerns the approach used to derive the governing equations for the LB method. If the LB method is viewed as a finite difference scheme, then it should be possible to derive the governing equations directly in terms of the model parameters (Δx, Δt, and τ) without the requirement that certain relations exist between these parameters. The second issue concerns numerical convergence of the LB scheme and its dependence on Δx, Δt, and τ. This can only be determined by deriving all of the leading order truncation error terms in terms of the model parameters and by comparing these terms with the error from numerical simulation.

This paper addresses the two key issues outlined above through a systematic derivation of the truncation error in terms of each of the relevant model parameters. The paper is organized as follows: The analysis begins in Section 2, where an expression for the intermediate variable f_j is derived directly in terms of an effective difference stencil for f_j^{eq}. With this effective stencil, a Taylor series expansion of f_j^{eq} on the nodes of the lattice is used to express f_j in differential form without the use of asymptotic expansions associated with the Chapman–Enskog method. These results are then used in Section 3 to provide the effective primitive variable difference stencils and truncation error for LB fluid models. The results are presented in one form assuming that τ is the independent parameter and in another assuming that Δt is the independent parameter. In Section 4, the analytical results of Section 3 are compared with numerical results for flows that have exact solutions. The important issues of consistency and convergence of the LB method are addressed in Section 5 by analyzing lattice Boltzmann as a finite difference method. From this analysis, conclusions are drawn regarding selections of the relaxation parameter, τ, and the discretization parameters Δx and Δt. Finally, the important role of boundary conditions on the convergence of LB is discussed in Section 6.

2. Taylor series analysis of the lattice Boltzmann equation

The first step in the analysis of the lattice Boltzmann equation is to obtain explicit expressions for the intermediate variables, f_j, solely in terms of the equilibrium quantities, f_j^{eq}. To this end, the discrete Boltzmann equation (Eq. (1)) is recast so that $f_j(\mathbf{x},t)$ appears on the left-hand side only,

$$f_j(\mathbf{x},t) = \left(1-\frac{1}{\tau}\right) f_j(\mathbf{x}-\Delta x\mathbf{w}_j, t-\Delta t) + \frac{1}{\tau} f_j^{\mathrm{eq}}(\mathbf{x}-\Delta x\mathbf{w}_j, t-\Delta t). \tag{2}$$

This expression is then applied recursively to eliminate f_j from the right-hand side of Eq. (2). This provides the difference representation for f_j in terms of f_j^{eq},

$$f_j(\mathbf{x},t) = \frac{1}{\tau}\sum_{n=1}^{\infty}\left(1-\frac{1}{\tau}\right)^{n-1} f_j^{\mathrm{eq}}(\mathbf{x}-n\Delta x\mathbf{w}_j, t-n\Delta t). \tag{3}$$

While Eq. (2) is the actual stencil, or pattern [16], used to calculate f_j, Eq. (3) is the pattern which expresses the dependencies of f_j upon the f_j^{eq}'s alone. Therefore, it is useful to define Eq. (3) as an effective stencil for f_j and to use this same terminology throughout the remaining analysis. The weights associated with each term in this effective stencil, relative to the weight of the nearest neighbor ($n=1$), are plotted versus n in Fig. 1 for various values of τ. For $\tau<1$, the weights of the surrounding neighbors alternate in sign and decay with the distance n. The rate of decay increases as $\tau \leftarrow 1$, and when $\tau=1$, the effective computational stencil contains contributions from only the nearest neighboring node ($n=1$). As τ increases past unity, the effective stencil again spreads, but with positive weights from each point in the effective stencil.

The next step in the analysis is to express f_j in differential form using a direct Taylor series expansion of f_j^{eq}:

$$f_j^{\mathrm{eq}}(\mathbf{x}-n\Delta x\mathbf{w}_j, t-n\Delta t) = f_j^{\mathrm{eq}}(\mathbf{x},t) + \sum_{m=1}^{\infty}\frac{1}{m!}\left[-n\Delta t\partial_t - n\Delta x\mathbf{w}_j\cdot\nabla\right]^m f_j^{\mathrm{eq}}(\mathbf{x},t), \tag{4}$$

where the notation ∂_t is used to denote time differentiation. Using this expansion in Eq. (3) yields

$$f_j(\mathbf{x},t) = \frac{1}{\tau}\sum_{n=1}^{\infty}\left(1-\frac{1}{\tau}\right)^{n-1} f_j^{\mathrm{eq}}(\mathbf{x},t) + \frac{1}{\tau}\sum_{m=1}^{\infty}\sum_{n=1}^{\infty}\left(1-\frac{1}{\tau}\right)^{n-1}\frac{(-n)^m}{m!}\left[\Delta t\partial_t + \Delta x\mathbf{w}_j\cdot\nabla\right]^m f_j^{\mathrm{eq}}(\mathbf{x},t). \tag{5}$$

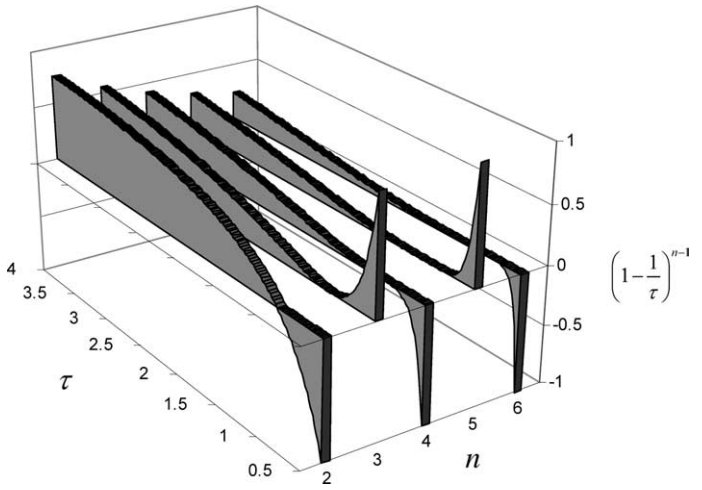

Fig. 1. Relative contributions to the effective f_j stencil from surrounding nodes.

Eq. (5) expresses f_j in terms of f_j^{eq} and its temporal and spatial gradients along the direction $\mathbf{w}_j$. This is written in a more convenient form as

$$f_j(\mathbf{x},t) = f_j^{\mathrm{eq}}(\mathbf{x},t) + \tau \sum_{m=1}^{\infty} \frac{p[\tau;m]}{m!} \left[\Delta t \partial_t + \Delta x \mathbf{w}_j \cdot \nabla\right]^m f_j^{\mathrm{eq}}(\mathbf{x},t), \tag{6}$$

where the infinite series $p[\tau;m]$ is defined as

$$p[\tau;m] \equiv \frac{1}{\tau^2} \sum_{n=1}^{\infty} \left(1-\frac{1}{\tau}\right)^{n-1} (-n)^m = \frac{(-1)^m}{\tau(\tau-1)} Li_{-m}\left[1-\frac{1}{\tau}\right]. \tag{7}$$

The notation $p[\tau;m]$ is used to denote that p is a continuous function of τ and is parameterized by the integer m. As indicated in Eq. (7), the infinite series in p is related to the polylogarithm function, Li. This series converges to a polynomial in τ of order $m-1$ for all m when $1/2 < \tau < \infty$. The identity $p[\tau;0] = 1/\tau$ has been used to simplify Eq. (6), and for $m = 1$ to 4,

$$p[\tau;1] = -1, \quad p[\tau;2] = 2\tau - 1, \tag{8}$$

$$p[\tau;3] = -6\tau^2 + 6\tau - 1, \quad p[\tau;4] = 24\tau^3 - 36\tau^2 + 14\tau - 1.$$

When $\tau = 1$, f_j is equal to f_j^{eq} from the previous time and location and $p[1;m] = (-1)^m$. The same results in Eqs. (6)–(8) can be obtained simply through expansion of the discrete propagator:

$$f_j(\mathbf{x},t) = \left[\frac{1}{1+\tau(\exp(D)-1)}\right] f_j^{\mathrm{eq}}(\mathbf{x},t), \tag{9}$$

where

$$D = \left[\Delta t \partial_t + \Delta x \mathbf{w}_j \cdot \nabla\right]. \tag{10}$$

Finally, it is necessary for the following analysis to note that the polynomials in Eq. (8) have roots at

$$\tau_2 = \frac{1}{2}, \quad \tau_3 = \frac{1}{2} + \frac{\sqrt{3}}{6} \approx 0.7887, \quad \tau_4 = \frac{1}{2} + \frac{\sqrt{6}}{6} \approx 0.9082, \tag{11}$$

where the subscripts of τ are used to denote the polynomials corresponding to each root.

The above results follow directly from a Taylor series analysis of the discrete Boltzmann equation. Unlike the Chapman–Enskog approach, this analysis does not require an assumed asymptotic relationship between f_j and f_j^{eq}. Also, the present approach does not require the introduction of multiple time scales or the collection of terms at matching orders [5].

It should also be noted that the above results are derived directly from the recursive application of the LB equation without incorporating the effects of initial or boundary conditions. For practical simulations, these results will only be realized when the initial and boundary conditions are consistent with the LB equation. To the degree that Eq. (6) is not satisfied by these conditions, the particle distribution will be modified, and the resulting macroscopic equations will contain additional error terms. Therefore, the accuracy of initial and boundary conditions is critically important, and this is specifically addressed in Section 6.

3. Taylor series analysis of lattice Boltzmann fluid models

3.1. Model description

In this section, the LB fluid models for both the square and hexagonal grids are examined. In order to accommodate the square grid (S) as shown in Fig. 2, it is useful to expand slightly the notation, $\mathbf{w}_j \rightarrow \mathbf{w}_{\sigma i}$, $f_j \rightarrow \mathrm{f}_{\sigma i}$, where σ is used to differentiate between diagonal ($\sigma = 2$) and Cartesian directions ($\sigma = 1$) and i is used to denote a specific direction. For generality, this same notation is used for the hexagonal grid (H) (Fig. 3), where σ is assigned the value 1 for all the vectors. Finally, f_0 is used for both grids to denote a value at each node corresponding to $\mathbf{w}_0 = \mathbf{0}$.

In LB models, primitive variables are updated from linear combinations of the intermediate variables, $f_{\sigma i}$. In this paper, the focus is on fluid transport, and the common moments for $f_{\sigma i}$ and $f_{\sigma i}^{\mathrm{eq}}$ are redefined as:

$$\rho = \sum_{\sigma i} f_{\sigma i} \quad \Rightarrow \quad p = c_{\mathrm{s}}^2 \sum_{\sigma i} f_{\sigma i} \quad \Rightarrow \quad \varsigma^2 \left(\frac{\Delta t^2}{\Delta x^2} \right) p = \sum_{\sigma i} f_{\sigma i}, \tag{12a}$$

$$\sum_{\sigma i} f_{\sigma i}^{\mathrm{eq}} = \rho \quad \Rightarrow \quad \sum_{\sigma i} f_{\sigma i}^{\mathrm{eq}} = \varsigma^2 \left(\frac{\Delta t^2}{\Delta x^2} \right) p, \tag{12b}$$

$$\rho u_\alpha = \sum_{\sigma i} f_{\sigma i} e_{\sigma i \alpha} \quad \Rightarrow \quad \rho u_\alpha = \left(\frac{\Delta x}{\Delta t} \right) \sum_{\sigma i} f_{\sigma i} w_{\sigma i \alpha}, \tag{13a}$$

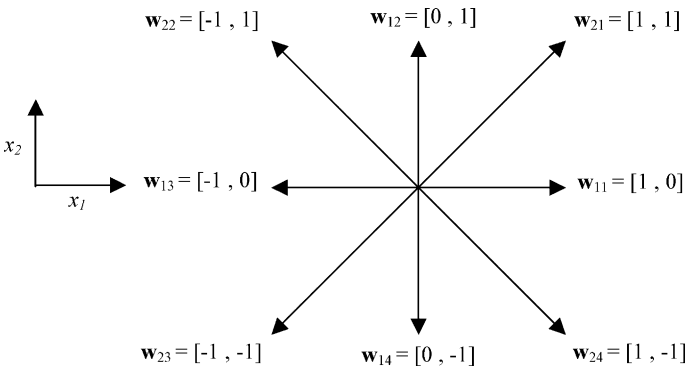

Fig. 2. Lattice directions associated with a square grid LB scheme.

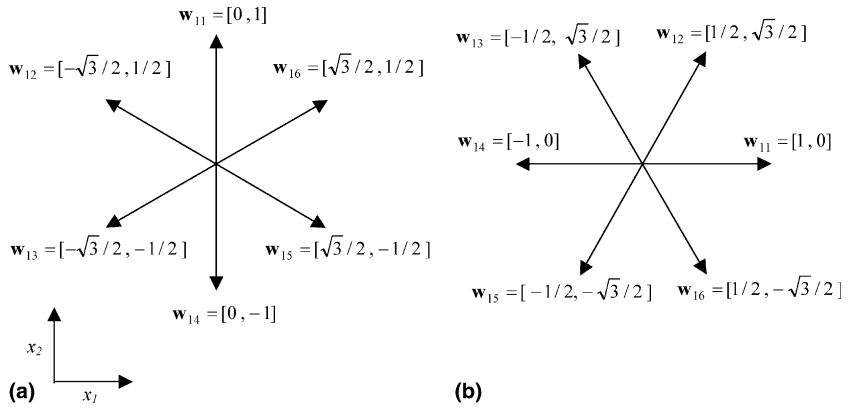

Fig. 3. Lattice directions associated with a hexagonal grid LB scheme.

$$\sum_{\sigma i} f_{\sigma i}^{\mathrm{eq}} e_{\sigma i\alpha} = \rho u_\alpha \;\Rightarrow\; \left(\frac{\Delta x}{\Delta t}\right)\sum_{\sigma i} f_{\sigma i}^{\mathrm{eq}} w_{\sigma i\alpha} = \rho u_\alpha, \tag{13b}$$

where $\mathbf{e}_{\sigma i} = c\mathbf{w}_{\sigma i}$ is commonly known as the microscopic velocity, c_s the speed of sound, ς is the ratio of the computational speed to the speed of sound ($\varsigma = c/c_s$), p is the pressure, u the velocity, and ρ is the density. Here, the equilibrium distributions are

$$f_{\sigma i}^{\mathrm{eq}} = \left(\frac{\Delta t^2}{\Delta x^2}\right)A_\sigma p + \left(\frac{\Delta t}{\Delta x}\right)B_\sigma w_{\sigma i\alpha}\rho u_\alpha + \left(\frac{\Delta t^2}{\Delta x^2}\right)C_\sigma w_{\sigma i\alpha}w_{\sigma i\beta}\rho u_\alpha u_\beta + \left(\frac{\Delta t^2}{\Delta x^2}\right)D_\sigma \rho u_\alpha u_\alpha. \tag{14}$$

Written this way, either the standard LB model (replacing p with ρc_s^2) or the so-called incompressible model of He and Luo [13] (ρ is a constant) can be recovered. The coefficients, $A_\sigma, B_\sigma, \ldots$, for both the hexagonal and square models are provided in Appendix A. It is worth noting that $\varsigma = \sqrt{3}$ corresponds to the typical choice [21] for this ratio and can be derived from the Maxwell–Boltzmann distribution function [14]. Using Eq. (3), which gives the effective stencil for $f_{\sigma i}$, the effective stencils for the primitive variables are obtained using the moment equations given in Eqs. (12a) and (13a):

$$\varsigma^2\left(\frac{\Delta t^2}{\Delta x^2}\right)p(\mathbf{x},t) = \frac{1}{\tau}\sum_{\sigma i}\sum_{n=1}^{\infty}\left(1-\frac{1}{\tau}\right)^{n-1} f_{\sigma i}^{\mathrm{eq}}(\mathbf{x} - n\Delta x\mathbf{w}_{\sigma i}, t - n\Delta t), \tag{15}$$

$$\rho u_\alpha(\mathbf{x},t) = \left(\frac{\Delta x}{\Delta t}\right)\frac{1}{\tau}\sum_{\sigma i}\sum_{n=1}^{\infty}\left(1-\frac{1}{\tau}\right)^{n-1} w_{\sigma i\alpha} f_{\sigma i}^{\mathrm{eq}}(\mathbf{x} - n\Delta x\mathbf{w}_{\sigma i}, t - n\Delta t). \tag{16}$$

These equations can be viewed as the effective difference stencils of the lattice Boltzmann model for fluid mechanics. They express the primitive variables in terms of other primitive variables at other locations and times via the definition of the equilibrium distribution (Eq. (14)). The effective pressure and x_1-momentum stencils for $\tau = 1$ on the square grid are provided in Appendix B.

3.2. Modified equations

To analyze the numerical accuracy and convergence properties of LB models, the modified equations must be examined. The term "modified equation" is reserved for the partial differential equation

approximated by the difference equations (Eqs. (15) and (16)). This includes both physically meaningful terms, i.e., the incompressible Navier–Stokes momentum equations, and numerical error terms representing the model error (compressibility) and truncation error. The process of introducing the definitions contained in Eq. (14) into Eqs. (15) and (16) and simplifying the results is shown in Appendix C. The physically meaningful terms that are produced correspond to the continuity and momentum equations. In order to recover the viscous term in the momentum equations the kinematic viscosity is expressed as

$$v = K_{\mathrm{S,H}} \frac{(2\tau - 1)\Delta x^2}{2\Delta t}; \quad K_{\mathrm{S}} = \frac{1}{3}, \quad K_{\mathrm{H}} = \frac{1}{4}. \tag{17}$$

The results shown and discussed here correspond to the so-called incompressible LB model of He and Luo [13]. The standard compressible model equations are also given in Appendix C. Also, to facilitate the analysis, it is useful to non-dimensionalize the continuity equations with

$$u^* = \frac{u}{U}, \quad x^* = \frac{x}{L}, \quad t^* = \frac{tU}{L}, \quad p^* = \frac{p}{\rho U^2}, \tag{18}$$

where U and L are the characteristic velocity and length, respectively. Here, pressure and time are non-dimensionalized using convective scales, which are most appropriate at high Reynolds numbers. Dropping the * notation, the non-dimensional conservation equations become

continuity:

$$\partial_\alpha u_\alpha = 0 + \mathrm{C.E.}, \tag{19}$$

momentum:

$$\partial_t u_\alpha + u_\beta \partial_\beta u_\alpha = -\partial_\alpha p + \frac{1}{Re} \partial_{\beta,\beta} u_\alpha + \mathrm{M.E.}, \tag{20}$$

where C.E. and M.E. are the model and truncation error of the continuity and momentum equations, respectively. Here Einstein notation is used and $\partial_\alpha = \partial/\partial x_\alpha$.

The truncation and model error can be expressed in two forms depending upon whether Δt or τ is considered the independent parameter in the viscosity relation (Eq. (17)). If τ is the independent parameter, then the continuity error is

$$\mathrm{C.E.} = -\Delta x^2 Re^2 (2\tau - 1)^2 \frac{K_{\mathrm{S,H}}^2 \varsigma^2}{4} \partial_t p + \mathrm{O}(\Delta x^4). \tag{21}$$

The first term on the right-hand side is the compressibility error. The truncation error in the momentum equation is

$$\begin{aligned} \mathrm{M.E.} = \Delta x^2 \Bigg[& Re(2\tau - 1)^2 \frac{K_{\mathrm{S,H}}(1 - 2K_{\mathrm{S,H}}\varsigma^2)}{4} \partial_\alpha (\partial_t p) + Re(2\tau - 1)^2 \frac{K_{\mathrm{S,H}}}{4} \partial_\beta (\partial_t u_\alpha u_\beta) \\ & + K_{\mathrm{S,H}} \frac{(-8\tau^2 + 8\tau - 1)}{4} \partial_{\beta,\beta} (\partial_t u_\alpha) + K_{\mathrm{S,H}} \frac{(-6\tau^2 + 6\tau - 1)}{2} \partial_{\alpha,\beta,\beta} \left(p - \frac{u_\lambda u_\lambda}{2} \right) \\ & + \frac{(-6\tau^2 + 6\tau - 1)}{6} C_{\alpha\beta\gamma\omega\lambda\eta} \partial_{\beta,\gamma,\omega} u_\lambda u_\eta + \frac{1}{Re} \frac{(12\tau^2 - 12\tau + 1)}{12 K_{\mathrm{S,H}}} B_{\alpha\beta\gamma\omega\lambda\eta} \partial_{\beta,\gamma,\omega,\eta} u_\lambda \Bigg] + \mathrm{O}(\Delta x^4), \end{aligned} \tag{22}$$

where the following notation has been introduced:

$$C_{\alpha\beta\gamma\omega\lambda\eta} = \sum_{\sigma i} C_\sigma w_{\sigma i\alpha} w_{\sigma i\beta} w_{\sigma i\gamma} w_{\sigma i\omega} w_{\sigma i\lambda} w_{\sigma i\eta}, \tag{23a}$$

$$B_{\alpha\beta\gamma\omega\lambda\eta} = \sum_{\sigma i} B_\sigma w_{\sigma i\alpha} w_{\sigma i\beta} w_{\sigma i\gamma} w_{\sigma i\omega} w_{\sigma i\lambda} w_{\sigma i\eta}. \tag{23b}$$

The polynomials in Eq. (22), $(2\tau-1)^2$, $(-6\tau^2+6\tau-1)$, and $(12\tau^2-12\tau+1)$, correspond to $p[\tau;2]^2$, $p[\tau;3]$, and $p[\tau;4]/p[\tau;2]$, respectively. The roots for the polynomials are given in Eq. (11). Plots of the polynomials are presented versus $(2\tau-1)$ in Fig. 4. These polynomials are significant because the choice of τ can strongly influence the size of each of the error terms in both Eqs. (21) and (22). The influence of τ on the error is investigated numerically and theoretically in Section 4 for steady and unsteady flows at various Reynolds numbers.

If Δt is considered as an independent variable in the error analysis, then the continuity and momentum errors are rewritten as

$$\text{C.E.} = -\frac{\Delta t^2}{\Delta x^2}\varsigma^2 \partial_t p + \mathrm{O}(\Delta t^2, \Delta x^4, (\Delta t/\Delta x)^4), \tag{24}$$

$$\begin{aligned}\text{M.E.} = {} & \frac{1}{Re}\frac{\Delta t^2}{\Delta x^2}\frac{(1-2K_{\mathrm{S,H}}\varsigma^2)}{K_{\mathrm{S,H}}}\partial_\alpha(\partial_t p) + \frac{1}{Re}\frac{\Delta t^2}{\Delta x^2}\frac{1}{K_{\mathrm{S,H}}}\partial_\beta(\partial_t u_\alpha u_\beta) + \left(\frac{K_{\mathrm{S,H}}\Delta x^2}{4} - \frac{2}{Re^2}\frac{\Delta t^2}{\Delta x^2}\frac{1}{K_{\mathrm{S,H}}}\right)\partial_{\beta,\beta}(\partial_t u_\alpha) \\ & + \left(\frac{K_{\mathrm{S,H}}\Delta x^2}{4} - \frac{3}{Re^2}\frac{\Delta t^2}{\Delta x^2}\frac{1}{K_{\mathrm{S,H}}}\right)\partial_{\alpha,\beta,\beta}\left(p - \frac{u_\lambda u_\lambda}{2}\right) + \left(\frac{\Delta x^2}{12} - \frac{1}{Re^2}\frac{\Delta t^2}{\Delta x^2}\frac{1}{K_{\mathrm{S,H}}^2}\right)C_{\alpha\beta\gamma\omega\lambda\eta}\partial_{\beta,\gamma,\omega}u_\lambda u_\eta \\ & + \frac{1}{ReK_{\mathrm{S,H}}}\left(\frac{1}{Re^2}\frac{\Delta t^2}{\Delta x^2}\frac{1}{K_{\mathrm{S,H}}^2} - \frac{\Delta x^2}{6}\right)B_{\alpha\beta\gamma\omega\lambda\eta}\partial_{\beta,\gamma,\omega,\eta}u_\lambda + \mathrm{O}(\Delta t^2, \Delta x^4, (\Delta t/\Delta x)^4),\end{aligned} \tag{25}$$

where Δt is the dimensionless time scaled with L/U. Written this way, the kinetic theory parameter,τ, has been eliminated and the truncation error is rigorously defined in terms of the discretization parameters Δx and Δt.

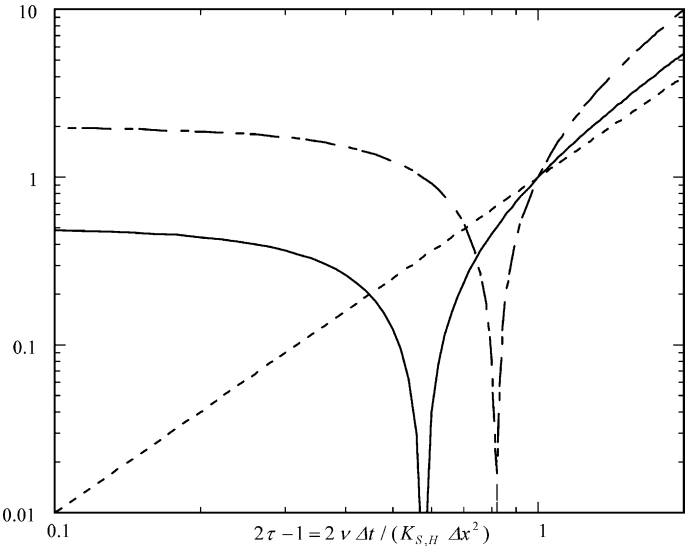

Fig. 4. Magnitudes of $(2\tau-1)^2$ (- - - - -), $(-6\tau^2+6\tau-1)$ (——) and $(12\tau^2-12\tau+1)$ (— — — —).

Again it is noted that the expressions for the truncation error given here are based on a high Reynolds number scaling. Written this way it appears that the error will diverge in the limit of zero Reynolds number. This is not the case, however, as could be shown using a low Reynolds number scaling. It is also noted that the ratio of the computational speed to the physical speed of sound, ζ, affects the error as shown in Eqs. (21) and (24) and the top lines of Eqs. (22) and (25). In the simulations below this parameter is simply chosen to be fixed at $\varsigma = \sqrt{7/3}$.

4. Numerical validation

In this section, two analytic flows are simulated to assess the truncation error analysis presented in the previous section. These simulations are performed under ideal conditions in which the boundary or initial conditions can be prescribed exactly.

4.1. Steady flows

The re-circulating Kovasznay flow [25] (plotted in Fig. 5) is simulated here at Reynolds numbers of 0.1 and 10.0 for various values of τ. The present study follows that of Noble et al. [31], in which the Kovasznay flow was employed to test LB boundary conditions for a square lattice. In their study, a variable density model was used. Here, the density is fixed [13] to eliminate compressibility effects, and the LB simulations are performed using a hexagonal lattice (oriented as in Fig. 3(a)).

The Kovasznay flow has an analytic solution as follows:

$$\begin{aligned}
\hat{u}_1(\mathbf{x}) &= U_0\left[1 - \exp\left(-\frac{\lambda x_1}{L}\right)\cos\left(\frac{2\pi x_2}{L}\right)\right],\\
\hat{u}_2(\mathbf{x}) &= -U_0\left[\frac{\lambda}{2\pi}\exp\left(-\frac{\lambda x_1}{L}\right)\sin\left(\frac{2\pi x_2}{L}\right)\right],\\
\hat{p}(\mathbf{x}) &= \frac{1}{2}\left[1 - \exp\left(-\frac{\lambda x_1}{L}\right)\right],
\end{aligned} \tag{26}$$

where

$$\lambda = \left[Re^2/4 + 4\pi^2\right]^{1/2} - Re/2 \tag{27}$$

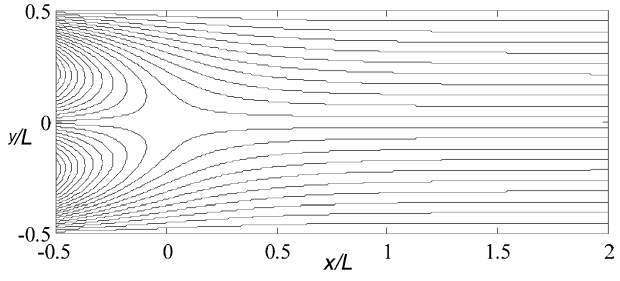

Fig. 5. Streamlines of the analytical solution to Kovasznay flow at $Re = 10.0$.

and the Reynolds number, Re, is given by

$$Re = \frac{U_0 L}{\nu}. \tag{28}$$

This flow is periodic at $x_2/L = \pm 1/2$ and requires boundary conditions only at two values of x_1. Following the study by Noble et al. [31], the same domain of $-1/2 \leqslant x_1/L \leqslant 2$ is simulated here.

At the boundaries of the x_1 numerical domain, there are two unknown $f_{\sigma i}$ for a hexagonal grid oriented as in Fig. 3(a). To determine these unknown quantities and the pressure at the boundaries, the boundary conditions of Noble et al. [30] are used. These conditions come from imposing the expressions for pressure (Eq. 12(a)) and momentum (Eq. 13(a)) at the boundaries. For the hexagonal grid, these constraints are sufficient and maintain the modified equations of the internal fluid.

Simulations are performed here using a hexagonal lattice with a 92×32 grid. For the simulations, the relative error is determined by

$$E1 = \frac{\sum_{x_1,x_2} \left| u_1 - \hat{u}_1 \right|}{\sum_{x_1,x_2} \left| \hat{u}_1 \right|} + \frac{\sum_{x_1,x_2} \left| u_2 - \hat{u}_2 \right|}{\sum_{x_1,x_2} \left| \hat{u}_2 \right|}. \tag{29}$$

This error is plotted in Fig. 6 for both the high and low Reynolds number simulations; the trends are similar to those from the analytical results in Fig. 4. For the $Re = 10.0$ simulations, the minimum error occurs at $\tau = 0.807 \pm 0.001$, while the root for $(6\tau^2 - 6\tau + 1)$ is at $\tau \approx 0.7889$. Additionally, when Figs. 6 and 4 are compared, the $(6\tau^2 - 6\tau + 1)$ variation in error becomes apparent. This result is consistent with the error analysis, which shows that the two dominant error terms at high Reynolds numbers are multiplied by $(6\tau^2 - 6\tau + 1)$ and the minimum should be at $\tau \approx 0.7889$. At $Re = 0.1$, the minimum in error occurs at $\tau = 0.907 \pm 0.001$, which is near the root of $(12\tau^2 - 12\tau + 1)$ at $\tau \approx 0.9082$. Again, when Figs. 6 and 4 are compared, the $(12\tau^2 - 12\tau + 1)$ variation in error appears. For this particular problem, the high Reynolds number error analysis successfully predicts that the minimum in error should lie at $\tau \approx 0.9082$. However, if a diffusive scaling is used, which is generally more appropriate at low Reynolds numbers, a pressure gradient term is apparent at the same order and is multiplied by $(6\tau^2 - 6\tau + 1)$.

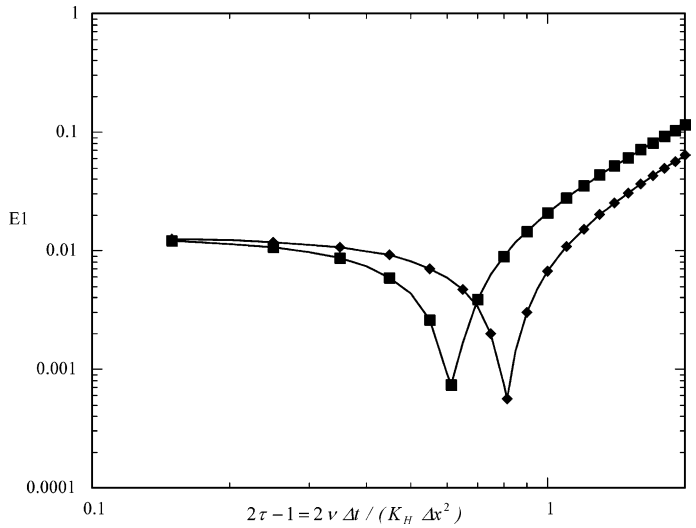

Fig. 6. Error for Kovasznay flow simulations on hexagonal grid with Noble et al.'s [22] consistent boundary conditions for $Re = 10.0$ (■) and $Re = 0.1$ (◆).

The same series of simulations has also been performed using both half and double the number of grid points. From these simulations, the error decreases quadratically with the number of points for any fixed value of τ. Similar convergence has been reported throughout the literature [6]. Finally, to test the analysis at higher Reynolds numbers, a limited series of simulations at $Re = 100$ have been performed on a fine grid of size 368×128. Results from these simulations demonstrate the same general trends in the error with τ as predicted for high Reynolds numbers and as found from the $Re = 10$ simulations. Additionally, a minimum in the error occurs at $\tau = 0.775 \pm 0.005$, which is near the predicted root of $\tau \approx 0.7889$ and the root for the $Re = 10$ simulation at $\tau = 0.807$.

4.2. Time-varying flows

Here, a translating shear flow is simulated at three Reynolds numbers for various values of τ. This study is motivated by the work of Skordos [34], where initial conditions were tested with this particular flow and several other time-varying flows.

Translating shear flow has the simple analytic solution

$$\begin{aligned} \hat{\boldsymbol{u}}_1(\mathbf{x}, t) &= U_1, \\ \hat{\boldsymbol{u}}_2(\mathbf{x}, t) &= U_2 \cos(kx_1 - kU_1 t) \exp(-k^2 \nu t). \end{aligned} \tag{30}$$

This flow has pure shear in the x_2-direction and a simple translation in the x_1-direction at a velocity of U_1. In his work, Skordos [34] chose $\nu = 1.0$, $U_2 = 1.0$, and $U_1 = 1.0$. Here, the first two choices are imposed and the third is relaxed in order to test a range of Reynolds numbers. The Reynolds number is therefore defined based upon U_1 as

$$Re_1 = \frac{L_1 U_1}{\nu}. \tag{31}$$

Skordos used a hexagonal grid oriented as in Fig. 3(b) and chose $k = 1$ so that $L_1 = 2\pi$. Simulations were performed on the domain $0 \leqslant x_1 \leqslant 2\pi$ and $0 \leqslant x_2 \leqslant \pi\sqrt{3}$ for an equal number of nodes in both directions. Since the flow is periodic, there is no need for boundary conditions but initial conditions must be prescribed carefully.

To obtain high accuracy initial conditions, $f_{\sigma i}$ is obtained from Eq. (6) and is evaluated through the fourth degree derivatives:

$$f_{\sigma i}(\mathbf{x}, t = 0) = f_{\sigma i}^{\mathrm{eq}}(\mathbf{x}, 0) + \tau \sum_{m=1}^{4} \frac{p[\tau; m]}{m!} [\Delta t \partial_t + \Delta x \mathbf{w}_{\sigma i} \cdot \nabla]^m f_{\sigma i}^{\mathrm{eq}}(\mathbf{x}, 0). \tag{32}$$

The exact temporal and spatial derivatives are then used in evaluating this expression. This approach is merely a higher order version of Skordos' [34] implementation of initial conditions.

Translating shear flow is simulated on a hexagonal grid with dimensions 30×30 for cross Reynolds numbers of zero (pure shear, no translation), 2π, and 20π. The relative error is determined at the time $t\nu k^2 = 1.0$, which corresponds to $t = 1.0$ for the parameters given above. This error is calculated as in Eq. (29), and when $U_1 = 0$ only the second term in Eq. (29) is evaluated. Simulation results at the three Reynolds numbers are plotted in Fig. 7. For the high Reynolds flow, $Re_1 = 20\pi$, the error decreases as $(2\tau - 1)^2$, or equivalently, with Δt^2. Again, this result is confirmed directly from the error analysis for high Reynolds number flows. At $Re_1 = 2\pi$, however a minimum begins to appear near the root of $(6\tau^2 - 6\tau + 1)$, which is $\tau \approx 0.7887$. For pure shear ($Re_1 = 0.0$) this root is quite clear. The minimum in error can be confirmed by the prior analysis but requires direct evaluation of each error term.

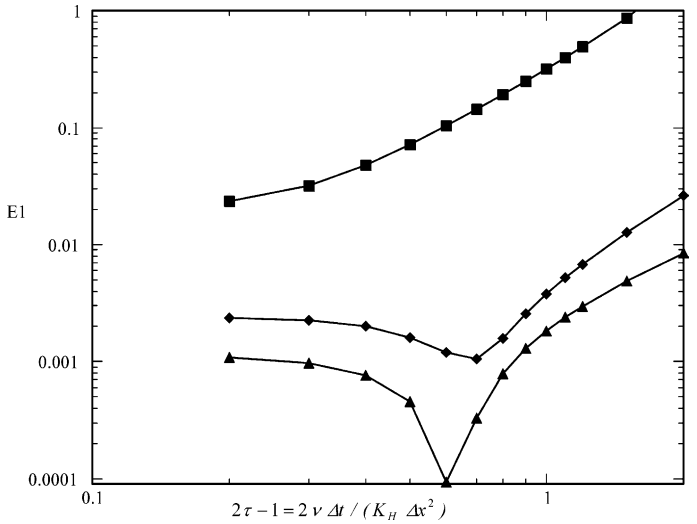

Fig. 7. Error for translating decaying shear flow, high accuracy initial conditions for $Re_1 = 20\pi$ (■), $Re_1 = 10\pi$ (◆), and $Re_1 = 0$ (▲).

5. Lattice Boltzmann as a finite difference method

5.1. Lattice Boltzmann ($\tau \neq 1$) versus nearest-neighbor centered differences ($\tau = 1$)

The analysis above allows comparison of the LB method for $\tau \neq 1$ to the nearest-neighbor finite difference scheme for $\tau = 1$. In this section, this comparison is performed by expanding upon the role of τ in the effective difference stencils given in Eqs. (15) and (16).

The LB fluid models should be considered first for $\tau = 1$. Again the effective difference stencils for this case are provided in Appendix B. Junk and Klar [23] provided a comprehensive analysis of how the differential operators are approximated by the individual finite difference stencils within Eqs. (B.2) and (B.4). Here, our focus is placed on the form of the effective x_1-momentum stencil. From the effective x_1-momentum stencil, the momentum for a node at time $t + \Delta t$ is determined largely as an average of the surrounding nodes' momenta from time t. This approach introduces artificial viscous terms (numerical diffusion error) and the kinematic viscosity is $\nu = K_{S,H}\Delta x^2/2\Delta t$. It is useful however, to note that this same formulation could be viewed as that of a typical centered difference scheme operating at the Courant–Friedrichs–Lewy limit for diffusion, $\Delta t \propto \Delta x^2/\nu$.

When τ is allowed to vary away from unity, the effective primitive variable difference stencils in Eqs. (15) and (16) extend further in space and time. As these effective stencils vary with τ, the derivative coefficients vary in the associated modified equations. Therefore this variation is found both in the viscous term and the error terms. For $\tau > 1$, the weights in the effective primitive variable stencils are of the same sign along any given direction and the derivative coefficients increase with the derivative degree and τ. For $\tau < 1$, the weights in the effective stencils oscillate about zero, which results in partial and eventually full cancellation of derivatives as the roots of the associated polynomials in τ are approached. However, it is not possible to minimize more than one order of derivative in any given simulation. Therefore, optimum choices can be made for τ only when the dominant error terms appear with the same order derivatives. This condition is satisfied in all cases for high Reynolds number flows. Again, for unsteady flows this optimum choice is $\tau = 1/2$ and for steady flows is $\tau \approx 0.7889$. For low Reynolds number flows, however, there is a spread in the derivative degrees of the leading error terms. The only exception to this rule is when there is steady

pure-shear flow. For this limiting case, the optimum choice is $\tau \approx 0.9089$. In general, it is wise to simply choose $\tau < 1$ for low Reynolds flows.

At this point it becomes clear that the LB model has higher accuracy for $\tau < 1$ when compared to the simpler nearest-neighbor finite difference scheme associated with $\tau = 1$. This increased accuracy is demonstrated in each of the simulations presented above. The higher accuracy is obtained in a manner similar to using leap-frog methods or wide difference stencils. However, unlike these other methods, only a few error terms can be eliminated in the LB model for any choice of τ. The implication of this constraint is that the formal order of the method remains the same and convergence with τ can be considered as hyper-convergence. This explains why the method still converges quadratically with the grid spacing for a given value of τ. However, hyper-convergence cannot be dismissed, which can be significant depending upon the Reynolds number.

The analysis and discussion above is consistent with other findings in literature. The preferred choice of operating in the "over-relaxation" regime ($\tau < 1$) for all flows is commonly accepted in the lattice Boltzmann community. Additionally, Swift et al. [36] found a minimum in "spurious velocities" near $\tau \approx 0.7889$ for their liquid-vapor LB model. Swift et al. also correctly noted that the next order error terms in their expansion are eliminated for this choice. In general, however, the choice of $\tau < 1$ has come in the past from kinetic theory or the "wave-number dependence of the evolution operator" [2]. Finally, it is worth noting that He et al. [15] found that the LB method reduces to a standard centered-difference solution for steady one-dimensional flows on a square grid. Therefore, for this special case, the error is independent of τ. The same expression for error can be obtained by manipulation of Eq. (22) for this special case.

5.2. Consistency and temporal accuracy

The direct Taylor series analysis from Section 3 can also be used to analyze the consistency and temporal accuracy of LB methods. Eqs. (24) and (25) describe the truncation error of LB for a given Δx and Δt. The relaxation time τ has been completely eliminated from these expressions using the definition of the kinematic viscosity so that the complete dependence of the error on the discretization parameters can be determined. From the leading-order truncation error terms, two major conclusions can be drawn. First, LB is formally second-order accurate in Δt for constant Δx. Second, the class of LB methods treated here remains consistent only if Δt decreases faster than Δx. Specifically, for the truncation error to vanish as the grid is refined, Eqs. (24) and (25) require that $\Delta t/\Delta x \to 0$ for the continuity equation and $\Delta t/(Re\Delta x) \to 0$ for the momentum equation. As described below, the methods typically used to satisfy these consistency requirements reduce the realizable accuracy of the method to first order in Δt. In terms of the dimensional lattice size and time step these requirements can be expressed as $U/(\Delta x/\Delta t) \to 0$ (from the continuity equation) and $(v/L)/(\Delta x/\Delta t) \to 0$ (from the momentum equation). The constraint on the consistency of the continuity equation is familiar to LB practitioners as the Mach number constraint. Here it has been shown that the fundamental basis for this Mach number constraint is the convergence criterion that Δt must decrease faster than Δx, as indicated by Eq. (24). The consistency requirement for the momentum equation can be stated that the computational speed $(\Delta x/\Delta t)$ must increase with refinement as compared to the diffusion speed (v/L).

It is worthwhile to mention the effect that the consistency constraint has on adaptively or a priori refined simulations using LB such as those found in literature [8,10,14,27]. In these simulations, a refined lattice region is patched with a coarse region in an effort to reduce the discretization error in regions of high gradients. In matching the solution across different grids, the viscosity and computational speed are typically held constant [10]. However, the truncation errors from Eqs. (24) and (25) clearly show that maintaining the same $\Delta x/\Delta t$ ratio as the grid is refined will not allow convergence to the Navier–Stokes equations. In practice, Fillapova and Hanel [10] were careful to constrain the value of $\tau < 1$ even for fine grids, but they also noted that this limits the degree of refinement that can be practically achieved. It is shown here that this constraint is based on the fact, that for steady or unsteady flows, a constant ratio

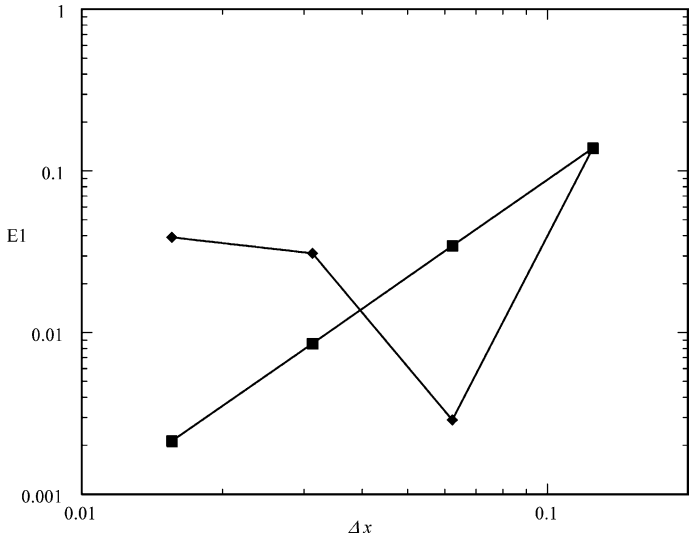

Fig. 8. Convergence for Kovasznay flow for $Re = 10.0$ on a hexagonal grid for $\Delta t/\Delta x^2$ constant (■) and $\Delta t/\Delta x$ constant (◆). The common point for the coarse grid corresponds to $\tau = 0.65$.

$\Delta x/\Delta t$ produces a constant error term that does not reduce with grid refinement. This point is demonstrated in Fig. 8 by plotting the error versus grid size for the Kovasznay flow for both constant $\Delta x/\Delta t$ and constant $\Delta x^2/\Delta t$. With constant $\Delta x/\Delta t$, the error decreases initially with grid refinement and then rises towards a constant value as the grid is refined further.

Lattice Boltzmann methods are similar to finite difference methods regarding the above consistency consideration. The relationship between LB and Dufort–Frankel discretizations was previously [1] pointed out for the diffusion equation. Both methods are consistent only if Δt decreases faster than Δx. Analysis of the Dufort–Frankel discretization [37] shows that one method of satisfying this consistency requirement is to insist that the quantity $\Delta t/\Delta x^2$ remain constant as the grid is refined, so that Δt decreases as Δx^2. If this specification is introduced into Eqs. (24) and (25), the terms of order $\Delta t^2/\Delta x^2$ become of order Δt. For fixed viscosity and fixed $\Delta t/\Delta x^2$, τ remains constant according to Eq. (30). Consequently, when refining the mesh with constant τ, LB discretizations are order Δt. This is in agreement with Reider and Sterling's [32] conclusions concerning the temporal accuracy of LB methods based on compressibility considerations. It is also important to note that at constant τ, LB methods are consistent. All terms in the truncation error vanish with Δt and Δx^2 for transient problems and Δx^2 for steady flows. This convergence is also demonstrated for the Kovasznay flow in Fig. 8.

In summary, the LB method is second-order accurate in time for fixed lattice spacing and is first order accurate in time and second-order accurate in space when refining the lattice spacing with constant τ. If the lattice spacing is reduced with a constant ratio $\Delta x/\Delta t$, LB is non-convergent. In this case, the error will reduce with mesh refinement until the $\Delta t^2/\Delta x^2$ term becomes dominant compared to the other terms which are either $O(\Delta x^2)$ or $O(\Delta t^2)$. Further decreasing the mesh size will not reduce the error.

6. Initial and boundary conditions

In the previous sections, the convergence of the LB method is examined assuming that $f_{\sigma i}$ extends infinitely in space and time. In this section, the convergence is examined for cases where additional truncation error is introduced via approximating initial or boundary conditions for $f_{\sigma i}$.

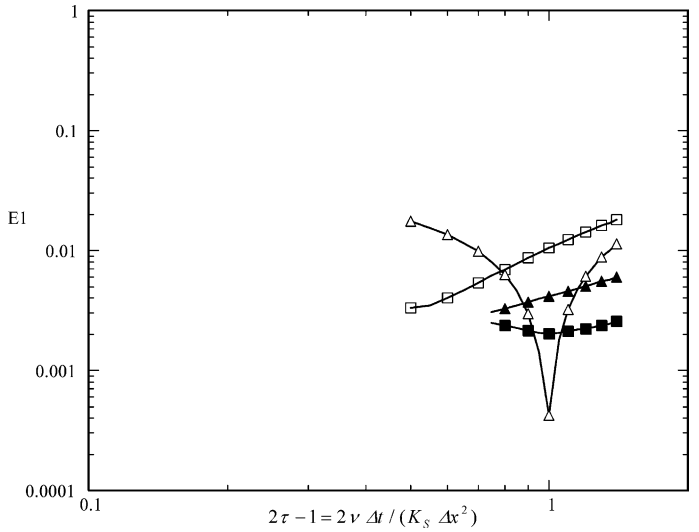

Fig. 9. Error for Kovasznay flow on square grid with third order extrapolation at $Re = 10.0$ (■), $Re = 0.1$ (▲) and with second-order extrapolation at $Re = 10.0$ (□), $Re = 0.1$ (△).

Over the years, a number of boundary condition formulations have been proposed based upon concepts such as bounce-back [24], numerical consistency [30], asymptotic expansions [34], and extrapolation [7,10,28]. Each of these boundary condition formulations has been shown to converge quadratically with grid size. However, numerical accuracy as a function of τ is also of interest, based upon the discussions in the previous sections. To demonstrate the influence of τ on accuracy, the Kovasznay flow from Section 4 is simulated on a square grid (80×32) with both second- and third-order extrapolation boundary conditions [7]. Specifically, these boundary conditions are

$$\begin{aligned} f_{\sigma i}(\mathbf{x},t) &= 2f_{\sigma i}(\mathbf{x}+\Delta x\mathbf{w}_{\sigma i}, t-\Delta t) - f_{\sigma i}(\mathbf{x}+2\Delta x\mathbf{w}_{\sigma i}, t-\Delta t), \\ f_{\sigma i}(\mathbf{x},t) &= 3f_{\sigma i}(\mathbf{x}+\Delta x\mathbf{w}_{\sigma i}, t-\Delta t) - 3f_{\sigma i}(\mathbf{x}+2\Delta x\mathbf{w}_{\sigma i}, t-\Delta t) + f_{\sigma i}(\mathbf{x}+3\Delta x\mathbf{w}_{\sigma i}, t-\Delta t). \end{aligned} \tag{33}$$

Results for the series of simulations are provided in Fig. 9. Results of the second-order extrapolation demonstrate that the choice of τ can have a large effect upon the accuracy. However, this is not the same hyper-convergence shown in Fig. 6. This difference shows that the boundary condition error can dominate the error of the interior fluid.

Skordos [34] simulated a number of time-varying flows including transient shear flow discussed above. In his work, Skordos derived boundary and initial conditions by expressing $f_{\sigma i}$ as $f_{\sigma i}^{\mathrm{eq}}$ plus leading order terms from what is equivalent to Eq. (6). Using the notation introduced in this paper, $f_{\sigma i}$ is expressed as

$$f_{\sigma i}(\mathbf{x}, t=0) = f_{\sigma i}^{\mathrm{eq}}(\mathbf{x},0) - \tau\Delta t\left(B_\sigma w_{\sigma i\alpha} w_{\sigma i\beta}\partial_\beta \rho u_\alpha - \frac{A_\sigma}{\varsigma^2}\partial_\alpha \rho u_\alpha\right)(\mathbf{x},0), \tag{34}$$

where the second term inside the brackets is obtained by replacing the time derivative of pressure. With this formulation, the spatial derivatives are obtained from finite difference approximations. This initial condition is used to simulate the translating shear flow from above on the hexagonal grid. Results for the simulations are provided in Fig. 10. These results compare well with those in Fig. 7 for the moderate and high Reynolds number flows. Therefore, it is accurate to say that hyper-convergence with τ is obtained for

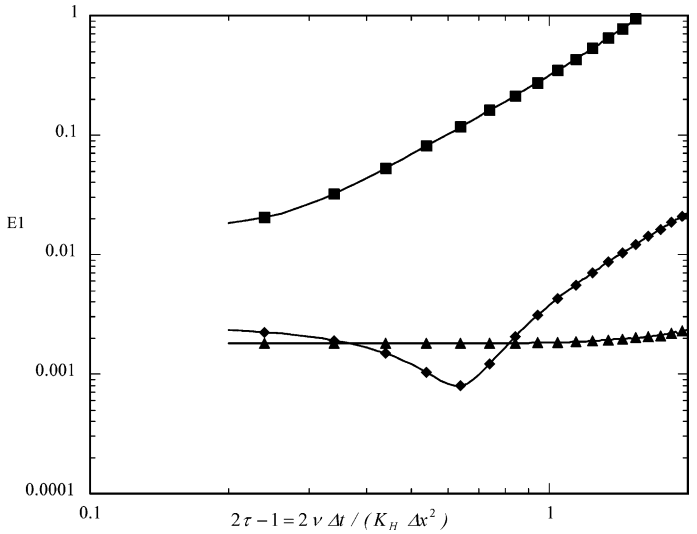

Fig. 10. Error for translating decaying shear flow on hexagonal grid with Skordos' [27] initial conditions for $Re_1 = 20\pi$ (■), $Re_1 = 10\pi$ (◆), and $Re = 0$ (▲).

this flow regime. In his work, Skordos [34] also finds hyper-convergence for the periodic decaying Taylor vortex. For this particular flow, the error decreases with $(2\tau - 1)^2$, or equivalently with Δt^2, for a fixed grid. Skordos also simulated a number of time-varying flows in which boundaries are also prescribed. Unfortunately, results for these flow simulations indicate that the hyper-convergence is lost again with the imposition of the boundary condition for velocity.

In summary, the accuracy of LB models depend considerably upon the choice of τ, and this dependence varies from model to model based upon boundary conditions. A Taylor series analysis needs to be performed for boundary conditions like that performed here for the internal fluid.

7. Conclusions

In this paper, a recursive application of the lattice Boltzmann (LB) equation is employed to obtain explicit forms for the effective primitive variable stencils in LB schemes. From these effective stencils, the modified equations for LB fluid flow models are obtained directly from Taylor series expansions. The truncation error, associated with the modified equations, is then expressed in two equivalent forms: one in terms of Δx and Δt and one in terms of Δx and the relaxation parameter τ. The analytical results are tested for both low and high Reynolds numbers through numerical simulation of steady 2-D Kovasznay flow and 1-D decaying shear flow.

When the modified equations are expressed solely in terms of τ and Δx, the error varies with the product of Δx^2 and low order polynomials in τ. When $\tau = 1$, the LB method is identical to a nearest-neighbor finite difference scheme with polynomials in τ of unit magnitude. When $\tau < 1$, the effective stencil extends in space and time with contributions that alter in sign. For optimal choices of τ (the roots of the polynomials), cancellation of error terms can occur, thereby resulting in hyper-convergence of the LB method. By scaling the modified equations appropriately, the truncation error varies as $(2\tau - 1)^2$ with a minimum at $\tau = 1/2$, or equivalently with Δt^2, for time-varying high Reynolds number flows. For steady high Reynolds number flows, the error varies as $(6\tau^2 - 6\tau + 1)$ with a minimum at $\tau \approx 0.7889$. This scaling breaks down for low Reynolds number flows, but a definite root appears at $\tau \approx 0.9082$ for steady shear flows, with the error varying as $(12\tau^2 - 12\tau + 1)$.

When the modified equations are written solely in terms of Δt and Δx, the LB method is second-order accurate in time for fixed lattice spacing and is first-order accurate in time and second-order accurate in space when refining with constant $\Delta x^2/\Delta t$. If the lattice spacing is reduced by maintaining a constant ratio $\Delta x/\Delta t$, the LB method does not converge. In this case, the error reduces with mesh refinement until the $\Delta t^2/\Delta x^2$ term becomes dominant compared to the other terms which are either $O(\Delta x^2)$ or $O(\Delta t^2)$. Further decreasing the mesh size does not reduce the error.

Finally, it is worth mentioning that the LB method has potential benefits over a standard explicit centered finite difference scheme for $\tau < 1$ due to hyper-convergence. However, these benefits are generally offset by the approximation of boundary conditions whose accuracy depends on τ.

Acknowledgements

The authors would like to acknowledge support by the National Science Foundation (Grant CTS-9521509) and by the National Computational Science Alliance in the form of a generous time allocation on the SGI Origin 2000 supercomputer. D.J.H. also acknowledges the support of the National Science Foundation, through a Graduate Fellowship and subsequent support by the NSF Sci. & Tech. Center of Advanced Materials for the Purification of Water with Systems (CAMPWS, cooperative agreement CTS-0120978). D.R.N. acknowledges the support of Sandia National Laboratories. Sandia is a multiprogram laboratory operated by Sandia Corporation, a Lockheed Martin Company, for the United States Department of Energy under Contract DE-AC04-94AL85000. We also thank an anonymous reviewer for suggesting the expansion in Eqs. (9) and (10).

Appendix A. Equilibrium distribution

An expression for the equilibrium distribution, $f_{\sigma i}^{\mathrm{eq}}$, is introduced in Eq. (14). Coefficients in this expression for the hexagonal grid are

$$\begin{aligned} &A_0 = \varsigma^2 - 2, \quad D_0 = -1, \\ &A_1 = \frac{1}{3}, \quad B_1 = \frac{1}{3}, \quad C_1 = \frac{2}{3}, \quad D_1 = -\frac{1}{6}. \end{aligned} \tag{A.1}$$

Coefficients for square grid are

$$\begin{aligned} &A_0 = \varsigma^2 - \frac{5}{3}, \quad D_0 = -\frac{2}{3}, \\ &A_1 = \frac{1}{3}, \quad B_1 = \frac{1}{3}, \quad C_1 = \frac{1}{2}, \quad D_1 = -\frac{1}{6}, \\ &A_2 = \frac{1}{12}, \quad B_2 = \frac{1}{12}, \quad C_2 = \frac{1}{8}, \quad D_2 = -\frac{1}{24}. \end{aligned} \tag{A.2}$$

Appendix B. Effective difference stencils for $\tau = 1$

The LB fluids model is a unique nearest-neighbor finite difference scheme when $\tau = 1$. For $\tau = 1$, Eq. (15) can be written as

$$\varsigma^2 p(\mathbf{x}, t) = \left(\frac{\Delta x^2}{\Delta t^2}\right) \sum_{\sigma i} f_{\sigma i}^{\mathrm{eq}}(\mathbf{x} - \Delta x \mathbf{w}_{\sigma i}, t - \Delta t). \tag{B.1}$$

For the square grid, this can be written as

$$\begin{aligned}\varsigma^2 p(\mathbf{x}, t+\Delta t) = \varsigma^2 p(\mathbf{x}, t) &+ \frac{\Delta x}{12\Delta t}\begin{bmatrix}1 & 0 & -1\\ 4 & 0 & -4\\ 1 & 0 & -1\end{bmatrix}\rho u_1(t) + \frac{\Delta x}{12\Delta t}\begin{bmatrix}-1 & -4 & -1\\ 0 & 0 & 0\\ 1 & 4 & 1\end{bmatrix}\rho u_2(t)\\ &+ \frac{1}{12}\begin{bmatrix}-1 & 0 & 1\\ -4 & 0 & 4\\ -1 & 0 & 1\end{bmatrix}p(t) + \frac{1}{4}\begin{bmatrix}-1 & 0 & 1\\ 0 & 0 & 0\\ 1 & 0 & -1\end{bmatrix}\rho u_1 u_2(t) + \frac{1}{12}\begin{bmatrix}1 & -2 & 1\\ 4 & -8 & 4\\ 1 & -2 & 1\end{bmatrix}\rho u_1^2(t)\\ &+ \frac{1}{12}\begin{bmatrix}1 & 4 & 1\\ -2 & -8 & -2\\ 1 & 4 & 1\end{bmatrix}\rho u_2^2(t). \end{aligned} \tag{B.2}$$

When $\tau = 1$, Eq. (16) is

$$\rho u_\alpha(\mathbf{x}, t) = \frac{\Delta x}{\Delta t}\sum_{\sigma i} f_{\sigma i}^{\mathrm{eq}}(\mathbf{x} - \Delta x \mathbf{w}_{\sigma i}, t - \Delta t). \tag{B.3}$$

The x_1-momentum equation is then

$$\begin{aligned}\rho u_1(\mathbf{x}, t+\Delta t) = &\frac{1}{12}\begin{bmatrix}1 & 0 & 1\\ 4 & 0 & 4\\ 1 & 0 & 1\end{bmatrix}\rho u_1(t) + \frac{1}{12}\begin{bmatrix}-1 & 0 & 1\\ 0 & 0 & 0\\ 1 & 0 & -1\end{bmatrix}\rho u_2(t) + \frac{\Delta t}{12\Delta x}\begin{bmatrix}1 & 0 & -1\\ 4 & 0 & -4\\ 1 & 0 & -1\end{bmatrix}p(t)\\ &+ \frac{\Delta t}{4\Delta x}\begin{bmatrix}-1 & 0 & -1\\ 0 & 0 & 0\\ 1 & 0 & 1\end{bmatrix}\rho u_1 u_2(t) + \frac{\Delta t}{12\Delta x}\begin{bmatrix}1 & 0 & -1\\ 4 & 0 & -4\\ 1 & 0 & -1\end{bmatrix}\rho u_1^2(t)\\ &+ \frac{\Delta t}{12\Delta x}\begin{bmatrix}1 & 0 & -1\\ -2 & 0 & 2\\ 1 & 0 & -1\end{bmatrix}\rho u_2^2(t). \end{aligned} \tag{B.4}$$

The individual stencils within Eqs. (B.2) and (B.4) were examined extensively by Junk and Klar [23].

Appendix C. Modified equations

Derivation of the modified equations for the LB fluid model is given below. The starting point is the Taylor series expansion of the effective stencil for f_j in Eq. (3), which yields Eq. (6). With the substitutions, $f_j \to f_{\sigma i}$ and $w_j \to w_{\sigma i}$, Eq. (6) is written as

$$f_{\sigma i} = f_{\sigma i}^{\mathrm{eq}} + \tau\sum_{m=1}^{\infty}\frac{p[\tau; m]}{m!}[\Delta t\partial_t + \Delta x \mathbf{w}_{\sigma i}\cdot\nabla]^m f_{\sigma i}^{\mathrm{eq}}. \tag{C.1}$$

This expression can be rewritten by expanding the terms of the Taylor series with the binomial theorem:

$$f_{\sigma i} = f_{\sigma i}^{\mathrm{eq}} + \tau\sum_{m=1}^{\infty}\frac{p[\tau; m]}{m!}\sum_{q=0}^{m}\frac{m!}{(m-q)!q!}[\Delta t\partial_t]^{m-q}[\Delta x \mathbf{w}_{\sigma i}\cdot\nabla]^q f_{\sigma i}^{\mathrm{eq}}. \tag{C.2}$$

For reasons that will be clear later, a factor of Δt is then brought out of the expansion,

$$f_{\sigma i} = f_{\sigma i}^{\mathrm{eq}} + \tau\Delta t\sum_{m=1}^{\infty}\sum_{q=0}^{m}\frac{p[\tau; m]}{(m-q)!q!}\Delta t^{m-q-1}\Delta x^q[\partial_t]^{m-q}[\mathbf{w}_{\sigma i}\cdot\nabla]^q f_{\sigma i}^{\mathrm{eq}}. \tag{C.3}$$

The presentation below uses a combination of vector and Einstein notation for the differential operators and other vector quantities. Writing the term corresponding to $m = 4$ and $q = 2$ in Einstein notation, for example, yields

$$[\partial_t]^2[\mathbf{w}_{\sigma i}\cdot\nabla]^2 f_{\sigma i}^{\mathrm{eq}} = \partial_{t,t}(\partial_{\alpha,\beta} f_{\sigma i}^{\mathrm{eq}}) w_{\sigma i\alpha} w_{\sigma i\beta} = \partial_{t,t,\alpha,\beta} f_{\sigma i}^{\mathrm{eq}} w_{\sigma i\alpha} w_{\sigma i\beta}. \tag{C.4}$$

The effective pressure and momentum stencils in Eqs. (15) and (16) come from moments of the effective stencil for $f_{\sigma i}$. Therefore, the Taylor series expansions for these effective stencils can be obtained from the moments of Eq. (C.3). The modified equation for the pressure is obtained from the zeroth moment of (C.3) and is written as

$$0 = \tau\Delta t \sum_{m=1}^{\infty}\sum_{q=0}^{m} \frac{p[\tau;m]}{(m-q)!q!}\Delta t^{m-q-1}\Delta x^q [\partial_t]^{m-q} \sum_{\sigma i}[\mathbf{w}_{\sigma i}\cdot\nabla]^q f_{\sigma i}^{\mathrm{eq}} \tag{C.5}$$

since the zeroth moment of $f_{\sigma i}^{\mathrm{eq}}$ equals the zeroth moment of $f_{\sigma i}$. Dividing through by $\tau\Delta t$ and explicitly expanding terms through $m = 1$ then produces

$$0 = -\partial_t \sum_{\sigma i} f_{\sigma i}^{\mathrm{eq}} - \partial_\alpha\left(\frac{\Delta x}{\Delta t}\right)\sum_{\sigma i} f_{\sigma i}^{\mathrm{eq}} w_{\sigma i\alpha} + \sum_{m=2}^{\infty}\sum_{q=0}^{m} \frac{p[\tau;m]}{(m-q)!q!}\Delta t^{m-q-1}\Delta x^q [\partial_t]^{m-q} \sum_{\sigma i}[\mathbf{w}_{\sigma i}\cdot\nabla]^q f_{\sigma i}^{\mathrm{eq}}. \tag{C.6}$$

Substituting in the definitions for the zeroth and first moments of $f_{\sigma i}^{\mathrm{eq}}$ (Eqs. (12b) and (13b)) and the general form for $f_{\sigma i}^{\mathrm{eq}}$ (Eq. (14)) provides

$$\begin{aligned} 0 = &-\varsigma^2\left(\frac{\Delta t^2}{\Delta x^2}\right)\partial_t p - \partial_\alpha \rho u_\alpha + \sum_{m=2}^{\infty}\sum_{q=0}^{m} \frac{p[\tau;m]}{(m-q)!q!}\Delta t^{m-q}\Delta x^{q-1}[\partial_t]^{m-q}\sum_{\sigma i}[\mathbf{w}_{\sigma i}\cdot\nabla]^q B_\sigma w_{\sigma i\alpha}\rho u_\alpha \\ &+ \sum_{m=2}^{\infty}\sum_{q=0}^{m}\left\{\frac{p[\tau;m]}{(m-q)!q!}\Delta t^{m-q+1}\Delta x^{q-2}[\partial_t]^{m-q}\sum_{\sigma i}[\mathbf{w}_{\sigma i}\cdot\nabla]^q\left(A_\sigma p + C_\sigma w_{\sigma i\alpha}w_{\sigma i\beta}\rho u_\alpha u_\beta + D_\sigma \rho u_\alpha u_\alpha\right)\right\}. \end{aligned} \tag{C.7}$$

This is the continuity equation for the LB method.

The modified equation for momentum is obtained by multiplying the first moment of Eq. (C.3) times $(\Delta x/\Delta t)$. This step results in the expression

$$0 = \left(\frac{\Delta x}{\Delta t}\right)\tau\Delta t \sum_{m=1}^{\infty}\sum_{q=0}^{m} \frac{p[\tau;m]}{(m-q)!q!}\Delta t^{m-q-1}\Delta x^q [\partial_t]^{m-q} \sum_{\sigma i}[\mathbf{w}_{\sigma i}\cdot\nabla]^q f_{\sigma i}^{\mathrm{eq}} w_{\sigma i\alpha} \tag{C.8}$$

since the first moment of $f_{\sigma i}^{\mathrm{eq}}$ equals the first moment of $f_{\sigma i}$. Taking this expansion through $m = 2$ and dividing by $\tau\Delta t$ provides

$$\begin{aligned} 0 = &-\partial_t\left(\frac{\Delta x}{\Delta t}\right)\sum_{\sigma i} f_{\sigma i}^{\mathrm{eq}} w_{\sigma i\alpha} - \partial_\beta\left(\frac{\Delta x^2}{\Delta t^2}\right)\sum_{\sigma i} f_{\sigma i}^{\mathrm{eq}} w_{\sigma i\alpha} w_{\sigma i\beta} + \frac{(2\tau-1)}{2}\partial_{t,t}\Delta x \sum_{\sigma i} f_{\sigma i}^{\mathrm{eq}} w_{\sigma i\alpha} \\ &+ \frac{(2\tau-1)}{2}\partial_{\beta,\gamma}\left(\frac{\Delta x^3}{\Delta t^2}\right)\sum_{\sigma i} f_{\sigma i}^{\mathrm{eq}} w_{\sigma i\alpha} w_{\sigma i\beta} w_{\sigma i\gamma} + (2\tau-1)\partial_{t,\beta}\frac{\Delta x^2}{\Delta t}\sum_{\sigma i} f_{\sigma i}^{\mathrm{eq}} w_{\sigma i\alpha} w_{\sigma i\beta} \\ &+ \sum_{m=3}^{\infty}\sum_{q=0}^{m} \frac{p[\tau;m]}{(m-q)!q!}\Delta t^{m-q-2}\Delta x^{q+1}[\partial_t]^{m-q}\sum_{\sigma i}[\mathbf{w}_{\sigma i}\cdot\nabla]^q f_{\sigma i}^{\mathrm{eq}} w_{\sigma i\alpha}. \end{aligned} \tag{C.9}$$

Again substituting in definition for the first moment of $f_{\sigma i}^{\mathrm{eq}}$ and the general form for $f_{\sigma i}^{\mathrm{eq}}$ (Eq. (14)) provides

$$\begin{aligned}0 = & -\partial_t \rho u_\alpha - \partial_\beta \sum_{\sigma i}\left(A_\sigma p + C_\sigma w_{\sigma i\gamma} w_{\sigma i\omega}\rho u_\gamma u_\omega + D_\sigma \rho u_\gamma u_\gamma\right) w_{\sigma i\alpha} w_{\sigma i\beta} + \frac{(2\tau-1)\Delta t}{2}\partial_{t,t}\rho u_\alpha + \frac{(2\tau-1)\Delta x^2}{2\Delta t}\partial_{\beta,\gamma} \\ & \times \sum_{\sigma i} B_\sigma w_{\sigma i\alpha} w_{\sigma i\beta} w_{\sigma i\gamma} w_{\sigma i\omega}\rho u_\omega + (2\tau-1)\Delta t\partial_{t,\beta}\sum_{\sigma i}\left(A_\sigma p + C_\sigma w_{\sigma i\gamma} w_{\sigma i\omega}\rho u_\gamma u_\omega + D_\sigma \rho u_\gamma u_\gamma\right) w_{\sigma i\alpha} w_{\sigma i\beta} \\ & + \sum_{m=3}^{\infty}\sum_{q=0}^{m}\frac{p[\tau;m]}{(m-q)!q!}\Delta t^{m-q-1}\Delta x^q [\partial_t]^{m-q}\sum_{\sigma i}[\mathbf{w}_{\sigma i}\cdot\nabla]^q B_\sigma w_{\sigma i\alpha} w_{\sigma i\beta}\rho u_\beta + \sum_{m=3}^{\infty}\sum_{q=0}^{m}\left\{\frac{p[\tau;m]}{(m-q)!q!}\right. \\ & \left.\times \Delta t^{m-q}\Delta x^{q-1}[\partial_t]^{m-q}\sum_{\sigma i}[\mathbf{w}_{\sigma i}\cdot\nabla]^q\left(A_\sigma p + C_\sigma w_{\sigma i\gamma} w_{\sigma i\omega}\rho u_\gamma u_\omega + D_\sigma \rho u_\gamma u_\gamma\right) w_{\sigma i\alpha}\right\}, \end{aligned} \tag{C.10}$$

where the fact that odd moments of $\mathbf{w}_{\sigma i}$ are zero has been imposed. The following are useful identities for the even moments of $\mathbf{w}_{\sigma i}$ on the square and hexagonal lattices:

Hexagonal:

$$\sum_i w_{\sigma i\alpha} w_{\sigma i\beta} = 3\delta_{\alpha\beta}, \quad \sum_i w_{\sigma i\alpha} w_{\sigma i\beta} w_{\sigma i\gamma} w_{\sigma i\omega} = 3/4\Delta_{\alpha\beta\gamma\omega}. \tag{C.11a}$$

Square:

$$\sum_i w_{\sigma i\alpha} w_{\sigma i\beta} = \begin{cases} 2\delta_{\alpha\beta}, & \sigma = 1, \\ 4\delta_{\alpha\beta}, & \sigma = 2, \end{cases} \quad \sum_i w_{\sigma i\alpha} w_{\sigma i\beta} w_{\sigma i\gamma} w_{\sigma i\omega} = \begin{cases} 2\delta_{\alpha\beta\gamma\omega}, & \sigma = 1, \\ 4\Delta_{\alpha\beta\gamma\omega} - 8\delta_{\alpha\beta\gamma\omega}, & \sigma = 2, \end{cases} \tag{C.11b}$$

$$\Delta_{\alpha\beta\gamma\omega} = \delta_{\alpha\beta}\delta_{\gamma\omega} + \delta_{\alpha\gamma}\delta_{\beta\omega} + \delta_{\alpha\omega}\delta_{\beta\gamma}, \quad \delta_{\alpha\beta\gamma\omega} = \begin{cases} 1, & \alpha = \beta = \gamma = \omega, \\ 0, & \text{otherwise.} \end{cases} \tag{C.12}$$

Using these identities, the momentum equation, Eq. (C.10), becomes

$$\begin{aligned}0 = & -\partial_t \rho u_\alpha - \partial_\beta \rho u_\alpha u_\beta - \partial_\alpha p + K_{\mathrm{S,H}}\frac{(2\tau-1)\Delta x^2}{2\Delta t}(\partial_{\beta,\beta}\rho u_\alpha + 2\partial_{\alpha,\beta}\rho u_\beta) + \Delta t\frac{(2\tau-1)}{2}\left\{\partial_t^2\rho u_\alpha + 2\partial_{t,\beta}(\rho u_\alpha u_\beta\right. \\ & \left. + p\delta_{\alpha\beta})\right\} + \sum_{m=3}^{\infty}\sum_{q=0}^{m}\frac{p[\tau;m]}{(m-q)!q!}\Delta t^{m-q-1}\Delta x^q[\partial_t]^{m-q}\sum_{\sigma i}[\mathbf{w}_{\sigma i}\cdot\nabla]^q B_\sigma w_{\sigma i\alpha} w_{\sigma i\beta}\rho u_\beta \\ & + \sum_{m=3}^{\infty}\sum_{q=0}^{m}\left\{\frac{p[\tau;m]}{(m-q)!q!}\Delta t^{m-q}\Delta x^{q-1}[\partial_t]^{m-q}\sum_{\sigma i}[\mathbf{w}_{\sigma i}\cdot\nabla]^q\left(A_\sigma p + C_\sigma w_{\sigma i\gamma} w_{\sigma i\omega}\rho u_\gamma u_\omega + D_\sigma \rho u_\gamma u_\gamma\right) w_{\sigma i\alpha}\right\}, \end{aligned} \tag{C.13}$$

where the coefficient $K_{\mathrm{S,H}}$ is specific to the grid. The coefficients for the square and hexagonal grid are

$$K_{\mathrm{S}} = \frac{1}{3}, \quad K_{\mathrm{H}} = \frac{1}{4}. \tag{C.14}$$

Eq. (C.13) is then a form of the Navier–Stokes equation if the kinematic viscosity is defined as

$$v = K_{\mathrm{S,H}}\frac{(2\tau-1)\Delta x^2}{2\Delta t}. \tag{C.15}$$

This expression reveals a relationship between the discretization parameters. Either Δt or τ can be eliminated from the truncation error using this expression. Using $\Delta t \to K_{\mathrm{S,H}}(2\tau-1)\Delta x^2/(2v)$ the continuity equation becomes

$$\begin{aligned}
0 = &-\Delta x^2 \varsigma^2 \frac{K_{\mathrm{S,H}}^2(2\tau-1)^2}{4v^2}\partial_t p - \partial_\alpha \rho u_\alpha + \sum_{m=2}^{\infty}\sum_{q=0}^{m}\left\{\frac{p[\tau;m]}{(m-q)!q!}\right.\\
&\times\left(\frac{K_{\mathrm{S,H}}(2\tau-1)}{2v}\right)^{m-q}\Delta x^{2m-q-1}[\partial_t]^{m-q}\sum_{\sigma i}[\mathbf{w}_{\sigma i}\cdot\nabla]^q B_\sigma w_{\sigma i\alpha}\rho u_\alpha\Big\} \quad (=0 \text{ for q even})\\
&+\sum_{m=2}^{\infty}\sum_{q=0}^{m}\left\{\frac{p[\tau;m]}{(m-q)!q!}\left(\frac{K_{\mathrm{S,H}}(2\tau-1)}{2v}\right)^{m-q+1}\Delta x^{2m-q}\right.\\
&\times[\partial_t]^{m-q}\sum_{\sigma i}[\mathbf{w}_{\sigma i}\cdot\nabla]^q\left(A_\sigma p + C_\sigma w_{\sigma i\alpha}w_{\sigma i\beta}\rho u_\alpha u_\beta + D_\sigma \rho u_\alpha u_\alpha\right)\Big\} \quad (=0 \text{ for } q \text{ odd}).
\end{aligned} \tag{C.16}$$

The same substitution into the momentum equation in Eq. (C.13) provides

$$\begin{aligned}
0 = &-\partial_t \rho u_\alpha - \partial_\beta \rho u_\alpha u_\beta - \partial_\alpha p + v(\partial_{\beta,\beta}\rho u_\alpha + 2\partial_{\alpha,\beta}\rho u_\beta) + \Delta x^2 K_{\mathrm{S,H}}\frac{(2\tau-1)^2}{4v}\left(\partial_t^2\rho u_\alpha + 2\partial_{t,\beta}(\rho u_\alpha u_\beta + p\delta_{\alpha\beta})\right)\\
&+\sum_{m=3}^{\infty}\sum_{q=0}^{m}\left\{\frac{p[\tau;m]}{(m-q)!q!}\left(\frac{K_{\mathrm{S,H}}(2\tau-1)}{2v}\right)^{m-q-1}\Delta x^{2m-q-2}\right.\\
&\times[\partial_t]^{m-q}\sum_{\sigma i}[\mathbf{w}_{\sigma i}\cdot\nabla]^q B_\sigma w_{\sigma i\alpha}w_{\sigma i\beta}\rho u_\beta\Big\} \quad (=0 \text{ for } q \text{ odd})\\
&+\sum_{m=3}^{\infty}\sum_{q=0}^{m}\left\{\frac{p[\tau;m]}{(m-q)!q!}\left(\frac{K_{\mathrm{S,H}}(2\tau-1)}{2v}\right)^{m-q}\Delta x^{2m-q-1}\right.\\
&\times[\partial_t]^{m-q}\sum_{\sigma i}[\mathbf{w}_{\sigma i}\cdot\nabla]^q\left(A_\sigma p + C_\sigma w_{\sigma i\gamma}w_{\sigma i\omega}\rho u_\gamma u_\omega + D_\sigma \rho u_\gamma u_\gamma\right)w_{\sigma i\alpha}\Big\} \quad (=0 \text{ for } q \text{ even}).
\end{aligned} \tag{C.17}$$

In the work presented above, there are no assumptions about the relative sizes of τ, Δx, or Δt. These expressions are valid for all ranges of these parameters. In order to consistently truncate these equations, however, the relative sizes of the error terms must be assessed. Each of these terms in Eqs. (C.16) and (C.17) can be written as $\mathrm{O}(\tau^r\Delta x^r)$, where r is a function of m and q. Formally, the ordering for these terms should be in terms of dimensionless quantities. However, while τ is already dimensionless, Δx is not. Therefore, it is assumed here that Δx is dimensionless with respect to a relevant length scale, and later this non-dimensionalization is introduced explicitly. As long as Δx vanishes at a rate significantly faster than τ grows, these terms may be considered to be $\mathrm{O}(\Delta x^r)$. This assumption is used now so that the leading order terms can be determined based solely on the associated powers of Δx. This assumption may be violated, however, when simulations are refined with $\Delta t = \Delta x$, which results in $\tau \to \Delta x^{-1}$. For this case, the truncation error below is still correct, but the relative ordering of the terms may not be. In other words, terms that would otherwise be insignificant, might be promoted and become dominant. The discussion in Section 5.1 clearly shows that this regime should be avoided, however. For the wide range of parameters for which this assumption is valid, identifying the leading order terms simply requires finding the maximum powers of Δx in the truncation error.

For Eq. (C.16), the first summation term is maximized when $(2m-q-1)$ is minimized and q is odd, and the second summation term is maximized when $(2m-q)$ is minimized and q is even. Truncating terms in Eq. (C.16) that are $\mathrm{O}(\Delta x^4)$ or higher yields

$$0 = -\partial_\alpha \rho u_\alpha - \Delta x^2 \varsigma^2 \frac{K_{\mathrm{S,H}}^2 (2\tau-1)^2}{4v^2}\partial_t p + \Delta x^2 K_{\mathrm{S,H}} \frac{(2\tau-1)^2}{2v}\partial_{t,\alpha}\sum_{\sigma i} B_\sigma w_{\sigma i\alpha} w_{\sigma i\beta}\rho u_\beta$$
$$+ \Delta x^2 K_{\mathrm{S,H}} \frac{(2\tau-1)^2}{4v}\partial_{\alpha,\beta}\sum_{\sigma i}\left(A_\sigma p + C_\sigma w_{\sigma i\gamma} w_{\sigma i\omega}\rho u_\gamma u_\omega + D_\sigma \rho u_\gamma u_\gamma\right) w_{\sigma i\alpha} w_{\sigma i\beta}$$
$$+ \Delta x^2 \frac{(-6\tau^2+6\tau-1)}{6}\partial_{\alpha,\beta,\gamma}\sum_{\sigma i} B_\sigma w_{\sigma i\alpha} w_{\sigma i\beta} w_{\sigma i\gamma} w_{\sigma i\omega}\rho u_\omega + \mathrm{O}(\Delta x^4). \tag{C.18}$$

Using the identities from Eqs. (C.11a), (C.11b) and (C.12) yields a simpler form for the continuity equation:

$$0 = -\partial_\alpha \rho u_\alpha + \Delta x^2 K_{\mathrm{S,H}} \frac{(-6\tau^2+6\tau-1)}{2}(\partial_{\beta,\beta,\alpha}\rho u_\alpha)$$
$$+ \Delta x^2 \frac{K_{\mathrm{S,H}}(2\tau-1)^2}{4v}\left\{-\frac{K_{\mathrm{S,H}}\varsigma^2}{v}\partial_t p + 2\partial_{t,\alpha}\rho u_\alpha + \partial_{\alpha,\beta}\left(p\delta_{\alpha,\beta} + \rho u_\alpha u_\beta\right)\right\} + \mathrm{O}(\Delta x^4). \tag{C.19}$$

Following the same procedure for Eq. (C.17), the first summation term is maximized when $(2m-q-2)$ is minimized and q is even, and the second summation term is maximized when $(2m-q-1)$ is minimized and q is odd. The modified momentum equation including the leading order terms is then

$$0 = -\partial_t \rho u_\alpha - \partial_\beta \rho u_\alpha u_\beta - \partial_\alpha p + v(\partial_{\beta,\beta}\rho u_\alpha + 2\partial_{\alpha,\beta}\rho u_\beta) + \Delta x^2 K_{\mathrm{S,H}}\frac{(2\tau-1)^2}{4v}\left(\partial_t^2 \rho u_\alpha + 2\partial_{t,\beta}(\rho u_\alpha u_\beta + p\delta_{\alpha\beta})\right)$$
$$+ \Delta x^2 \frac{(-6\tau^2+6\tau-1)}{6}\left\{3\partial_{t,\beta,\gamma}\sum_{\sigma i} B_\sigma w_{\sigma i\alpha} w_{\sigma i\beta} w_{\sigma i\gamma} w_{\sigma i\omega}\rho u_\omega + \partial_{\beta,\gamma,\omega}\sum_{\sigma i}(A_\sigma p + C_\sigma w_{\sigma i\lambda} w_{\sigma i\eta} u_\lambda u_\eta\right.$$
$$\left. + D_\sigma u_\lambda u_\lambda) w_{\sigma i\alpha} w_{\sigma i\beta} w_{\sigma i\gamma} w_{\sigma i\omega}\right\} + \Delta x^2 v \frac{(12\tau^2-12\tau+1)}{12K_{\mathrm{S,H}}}$$
$$\times \partial_{\beta,\gamma,\omega,\lambda}\sum_{\sigma i} B_\sigma w_{\sigma i\alpha} w_{\sigma i\beta} w_{\sigma i\gamma} w_{\sigma i\omega} w_{\sigma i\lambda} w_{\sigma i\eta}\rho u_\eta + \mathrm{O}(\Delta x^4). \tag{C.20}$$

Using the identities in Eqs. (C.11a), (C.11b) and (C.12) provides a simpler form of the momentum equation

$$0 = -\partial_t \rho u_\alpha - \partial_\beta \rho u_\alpha u_\beta - \partial_\alpha p + v(\partial_{\beta,\beta}\rho u_\alpha + 2\partial_{\alpha,\beta}\rho u_\beta) + \Delta x^2 K_{\mathrm{S,H}}\frac{(2\tau-1)^2}{4v}\left\{\partial_t^2 \rho u_\alpha + 2\partial_{t,\beta}(\rho u_\alpha u_\beta + p\delta_{\alpha,\beta})\right\}$$
$$+ \Delta x^2 \frac{(-6\tau^2+6\tau-1)}{2}\left\{K_{\mathrm{S,H}}\partial_t(\partial_{\beta,\beta}\rho u_\alpha + 2\partial_{\alpha,\beta}\rho u_\beta) + K_{\mathrm{S,H}}\partial_{\alpha,\beta,\beta}\left(p - \frac{\rho u_\gamma u_\gamma}{2}\right)\right.$$
$$\left. + \frac{1}{3}C_{\alpha\beta\lambda\gamma\omega\eta}\partial_{\beta,\gamma,\omega}\rho u_\lambda u_\eta\right\} + \Delta x^2 v\frac{(12\tau^2-12\tau+1)}{12K_{\mathrm{S,H}}}B_{\alpha\beta\lambda\gamma\omega\eta}\partial_{\beta,\gamma,\omega,\eta}\rho u_\eta + \mathrm{O}(\Delta x^4), \tag{C.21}$$

where

$$B_{\alpha\beta\gamma\omega\lambda\eta} = \sum_{\sigma i} B_\sigma w_{\sigma i\alpha} w_{\sigma i\beta} w_{\sigma i\gamma} w_{\sigma i\lambda} w_{\sigma i\omega} w_{\sigma i\eta}, \tag{C.22a}$$

$$C_{\alpha\beta\lambda\gamma\omega\eta} = \sum_{\sigma i} C_\sigma w_{\sigma i\alpha} w_{\sigma i\beta} w_{\sigma i\gamma} w_{\sigma i\lambda} w_{\sigma i\omega} w_{\sigma i\eta}. \tag{C.22b}$$

To further simplify the continuity and momentum equations in Eqs. (C.19) and (C.21), these equations can be combined to eliminate undesirable terms in the truncation error.

Eq. (C.19) can first be simplified by applying Eq. (C.21) to eliminate the third term on the second line of Eq. (C.19). Specifically,

$$\begin{aligned} 0 &= C19 + \Delta x^2 K_{\mathrm{S,H}} \frac{(2\tau-1)^2}{4\nu} \nabla(C21) \\ &= -\partial_\alpha \rho u_\alpha + \Delta x^2 \frac{K_{\mathrm{S,H}}}{4} (\partial_{\beta,\beta,\alpha} \rho u_\alpha) + \Delta x^2 \frac{K_{\mathrm{S,H}}(2\tau-1)^2}{4\nu} \left\{ -\frac{K_{\mathrm{S,H}} \varsigma^2}{\nu} \partial_t p + \partial_{t,\alpha} \rho u_\alpha \right\} + \mathrm{O}(\Delta x^4). \end{aligned} \tag{C.23}$$

This equation can be further simplified then since,

$$\begin{aligned} 0 &= C23 + \Delta x^2 K_{\mathrm{S,H}} \frac{(2\tau-1)^2}{4\nu} \partial_t (C23) + \Delta x^2 \frac{K_{\mathrm{S,H}}}{4} \nabla^2 (C23) \\ &= -\partial_\alpha \rho u_\alpha - \Delta x^2 \varsigma^2 \frac{K_{\mathrm{S,H}}^2 (2\tau-1)^2}{4\nu^2} \partial_t p + \mathrm{O}(\Delta x^4). \end{aligned} \tag{C.24}$$

The continuity equations are then

$$\rho \text{ constant}: \quad \partial_\alpha u_\alpha = -\frac{\Delta x^2}{\rho} \varsigma^2 \frac{K_{\mathrm{S,H}}^2 (2\tau-1)^2}{4\nu^2} (\partial_t p) + \mathrm{O}(\Delta x^4) \tag{C.25}$$

$$\rho \text{ varying}: \quad \partial_\alpha u_\alpha = -\frac{\Delta x^2}{\rho} \varsigma^2 \frac{K_{\mathrm{S,H}}^2 (2\tau-1)^2}{4\nu^2} (\partial_t p + u_\alpha \partial_\alpha p) + \mathrm{O}(\Delta x^4). \tag{C.26}$$

This first result is used for the error analysis in the main text. In a similar fashion, Eq. (C.21) can be simplified using

$$\begin{aligned} 0 &= C21 + 2\nu \nabla(C24) + \Delta x^2 K_{\mathrm{S,H}} (-6\tau^2 + 6\tau - 1) \nabla \partial_t (C24) \\ &= -\partial_t \rho u_\alpha - \partial_\beta \rho u_\alpha u_\beta - \partial_\alpha p + \nu \partial_{\beta,\beta} \rho u_\alpha + \Delta x^2 K_{\mathrm{S,H}} \frac{(2\tau-1)^2}{4\nu} \{ -2K_{\mathrm{S,H}} \zeta^2 \partial_\alpha (\partial_t p) + \partial_t^2 \rho u_\alpha \\ &\quad + 2\partial_{t,\beta} (\rho u_\alpha u_\beta + p\delta_{\alpha,\beta}) \} + \Delta x^2 \frac{(-6\tau^2 + 6\tau - 1)}{2} \left\{ K_{\mathrm{S,H}} \partial_{\beta,\beta} (\partial_t \rho u_\alpha) + K_{\mathrm{S,H}} \partial_{\alpha,\beta,\beta} \left(p - \frac{\rho u_\gamma u_\gamma}{2} \right) \right. \\ &\quad \left. + \frac{1}{3} C_{\alpha\beta\lambda\gamma\omega\eta} \partial_{\beta,\gamma,\omega} \rho u_\lambda u_\eta \right\} + \Delta x^2 \nu \frac{(12\tau^2 - 12\tau + 1)}{12 K_{\mathrm{S,H}}} B_{\alpha\beta\lambda\gamma\omega\eta} \partial_{\beta,\gamma,\omega,\eta} \rho u_\eta + \mathrm{O}(\Delta x^4). \end{aligned} \tag{C.27}$$

A final combination provides

$$\begin{aligned} 0 &= C27 + \Delta x^2 \frac{K_{\mathrm{S,H}}}{\nu} \frac{(2\tau-1)^2}{4} \partial_t (C27) = -\partial_t \rho u_\alpha - \partial_\beta \rho u_\alpha u_\beta - \partial_\alpha p + \nu \partial_{\beta,\beta} \rho u_\alpha \\ &\quad + \Delta x^2 K_{\mathrm{S,H}} \frac{(2\tau-1)^2}{4\nu} \{ (1 - 2K_{\mathrm{S,H}} \zeta^2) \partial_\alpha (\partial_t p) + \partial_\beta (\partial_t \rho u_\alpha u_\beta) \} + \Delta x^2 K_{\mathrm{S,H}} \frac{(-8\tau^2 + 8\tau - 1)}{4} \partial_{\beta,\beta} (\partial_t \rho u_\alpha) \\ &\quad + \Delta x^2 \frac{(-6\tau^2 + 6\tau - 1)}{2} \left\{ K_{\mathrm{S,H}} \partial_{\alpha,\beta,\beta} \left(p - \frac{\rho u_\gamma u_\gamma}{2} \right) + \frac{1}{3} C_{\alpha\beta\lambda\gamma\omega\eta} \partial_{\beta,\gamma,\omega} \rho u_\lambda u_\eta \right\} \\ &\quad + \Delta x^2 \nu \frac{(12\tau^2 - 12\tau + 1)}{12 K_{\mathrm{S,H}}} B_{\alpha\beta\lambda\gamma\omega\eta} \partial_{\beta,\gamma,\omega,\eta} \rho u_\eta + \mathrm{O}(\Delta x^4). \end{aligned} \tag{C.28}$$

The momentum equations are then

$$\rho \text{ constant}: \quad \partial_t u_\alpha + u_\beta \partial_\beta u_\alpha = -\frac{1}{\rho}\partial_\alpha p + \nu \partial_{\beta,\beta} u_\alpha + \frac{1}{\rho}\text{T.E.} \tag{C.29}$$

$$\rho \text{ varying}: \quad \partial_t u_\alpha + u_\beta \partial_\beta u_\alpha = -\frac{1}{\rho}\partial_\alpha p + \nu \partial_{\beta,\beta} u_\alpha + \frac{\nu}{\rho c_s^2}\Big(u_\alpha \partial_{\beta,\beta} p + (\partial_\beta u_\alpha)(\partial_\beta p)\Big) + \frac{1}{\rho}\text{T.E.} \tag{C.30}$$

The truncation error, T.E. is the last three lines of Eq. (C.28) and is presented in the main body of the text.

In the main body of the text, the continuity and momentum equations are presented in dimensionless form for ρ constant. When ρ is variable, one obtains the following dimensionless conservation equations when τ is considered the independent variable:

$$\partial_\alpha u_\alpha = -\Delta x^2 Re^2 (2\tau - 1)^2 \frac{K_{S,H}^2 \varsigma^2}{4\rho}(\partial_t p + u_\alpha \partial_\alpha p) + O(\Delta x^4), \tag{C.31}$$

$$\partial_t u_\alpha + u_\beta \partial_\beta u_\alpha = -\partial_\alpha p + \frac{1}{Re}\partial_{\beta,\beta} u_\alpha + \frac{Re\Delta x^2}{\rho} K_{S,H}^2 \varsigma^2 \frac{(2\tau - 1)^2}{4}\big(u_\alpha \partial_{\beta,\beta} p + (\partial_\beta u_\alpha)(\partial_\beta p)\big) + \frac{1}{\rho}\text{M.E.} \tag{C.32}$$

The momentum error, M.E., is only a slight variation of that presented in the main text for ρ constant.

References

[1] M.G. Ancona, Fully-Lagrangian and lattice Boltzmann methods for solving systems of conservation equations, J. Comput. Phys. 115 (1994) 107.
[2] O. Behrend, R. Harris, P.B. Warren, Hydrodynamic behavior of lattice Boltzmann and lattice Bhatnagar–Gross–Krook models, Phys. Rev. E 50 (1994) 4586.
[3] R. Benzi, S. Succi, M. Vergassola, The lattice Boltzmann equation: theory and applications, Phys. Rep. 22 (1992) 145.
[4] P. Bhatnagar, E.P. Gross, M.K. Krook, A model for collision processes in gases. I. Small amplitude processes in charged an neutral one-component systems, Phys. Rev. 94 (1954) 511.
[5] H. Chen, S. Chen, W.H. Matthaeus, Recovery of Navier–Stokes equations using a lattice-gas Boltzmann method, Phys. Rev. E 45 (1992) R5339.
[6] S. Chen, G.D. Doolen, Lattice Boltzmann method for fluid flows, Annu. Rev. Fluid. Mech. 30 (1998) 329.
[7] S. Chen, D. Martinez, On boundary conditions in lattice Boltzmann methods, Phys. Fluids 8 (1996) 2527.
[8] A. Dupuis, B. Chopard, Theory and applications of an alternative lattice Boltzmann grid refinement algorithm, Phys. Rev. E 67 (2003) 066707.
[9] B.H. Elton, Comparisons of lattice Boltzmann and finite difference methods for a two-dimensional viscous Burgers equation, SIAM J. Sci. Comput. 17 (1996) 783.
[10] O. Filippova, D. Hanel, Grid refinement for lattice-BGK models, J. Comput. Phys. 147 (1998) 219.
[11] U. Frisch, B. Hasslacher, Y. Pomeau, Lattice-gas automata for the Navier–Stokes equation, Phys. Rev. Lett. 56 (1986) 1505.
[12] A.K. Gunstensen, D.H. Rothman, S. Zaleski, G. Zanetti, Lattice Boltzmann model of immiscible fluids, Phys. Rev. A 43 (1991).
[13] X. He, L.S. Luo, Lattice Boltzmann model for the incompressible Navier–Stokes equation, J. Stat. Phys. 88 (1997) 927.
[14] X. He, L.S. Luo, A priori derivation of the lattice Boltzmann equation, Phys. Rev. E 55 (1997) 115.
[15] X. He, Q. Zou, L.S. Luo, Analytic solutions of simple flows and analysis of nonslip boundary conditions for the lattice Boltzmann BGK model, J. Stat. Phys. 87 (1997) 115.
[16] M.T. Heath, Scientific Computing: An Introductory Survey, McGraw-Hill, New York, 1997.
[17] F.J. Higuera, J. Jimenez, Boltzmann approach to lattice gas simulations, Europhys. Lett. 8 (1989) 517.
[18] F.J. Higuera, S. Succi, Simulating the flow around a circular cylinder with a lattice Boltzmann equation, Europhys. Lett. 8 (1989) 517.
[19] F.J. Higuera, S. Succi, R. Benzi, Lattice gas-dynamics with enhanced collisions, Europhys. Lett. 9 (1989) 345.
[20] D.J. Holdych, J.G. Georgiadis, R.O. Buckius, Migration of a van der Waals bubble: Lattice Boltzmann formulation, Phys. Fluids 13 (2001) 817.
[21] S. Hou, Q. Zou, S. Chen, G. Doolen, A.C. Cogley, Simulation of cavity flow by the Lattice Boltzmann method, J. Comput. Phys. 118 (1995) 329.

[22] M. Junk, A finite difference interpretation of the lattice Boltzmann method, Numer. Methods Partial Differential Equations 17 (2001) 383.
[23] M. Junk, A. Klar, Discretizations for the incompressible Navier–Stokes equations based on the lattice Boltzmann method, SIAM J. Sci. Comp. 22 (2000) 1.
[24] I.C. Kim, Second order bounce back boundary condition for the lattice-Boltzmann fluid simulation, KSME Int. J. 14 (2000) 84.
[25] L.I.G. Kovasznay, Laminar flow behind a two-dimensional grid, Proc. Camb. Philos. Soc. 48 (1948).
[26] A. Ladd, Numerical simulations of particle suspensions via a discretized Boltzmann equation. Part 2. Numerical results, J. Fluid Mech. 271 (1994) 311.
[27] C.L. Lin, Y.G. Lai, Lattice Boltzmann method on composite grids, Phys. Rev. E 62 (2000) 2219.
[28] R.S. Maier, R.S. Bernard, D.W. Grunau, Boundary conditions for the lattice Boltzmann method, Phys. Fluids 8 (1996) 1788.
[29] G.R. McNamara, G. Zanetti, Use of the Boltzmann equation to simulate lattice-gas automata, Phys. Rev. Lett. 61 (1988) 2332.
[30] D. Noble, S. Chen, J.G. Georgiadis, R.O. Buckius, A consistent hydrodynamic boundary condition for lattice Boltzmann methods, Phys. Fluids 7 (1995) 203.
[31] D. Noble, J.G. Georgiadis, R.O. Buckius, Direct assessment of lattice-Boltzmann simulations of recirculating flow, J. Stat. Phys. 81 (1995) 17.
[32] M.B. Reider, J.D. Sterling, Accuracy of discrete-velocity BGK models for the simulation of the incompressible Navier–Stokes equations, Comp. Fluids 24 (1995) 459.
[33] X. Shan, H. Chen, Lattice Boltzmann model for simulating flows with multiple phases and components, Phys. Rev. E 47 (1993) 1815.
[34] P.A. Skordos, Initial and boundary conditions for the lattice Boltzmann method, Phys. Rev. E 48 (1993) 4823.
[35] S. Succi, E. Foti, F.J. Higuera, 3-Dimensional flows in complex geometries with the lattice Boltzmann Method, Europhys. Lett. 10 (1989) 433.
[36] M.R. Swift, E. Orlandini, W.R. Osborn, J.M. Yeomans, Lattice Boltzmann simulations of liquid-gas and binary fluid systems, Phys. Rev. E 54 (1996) 5041.
[37] J.C. Tannehill, D.A. Anderson, R.H. Pletcher, Computational Fluid Mechanics and Heat Transfer, Taylor & Francis, Washington, DC, 1997.